UC-25

LBL-6612 c.1

CHARACTERIZATION OF SIALON-TYPE MATERIALS

Paul Newman Spencer
(M. S. thesis)

June 1977

Prepared for the U. S. Energy Research and
Development Administration under Contract W-7405-ENG-48

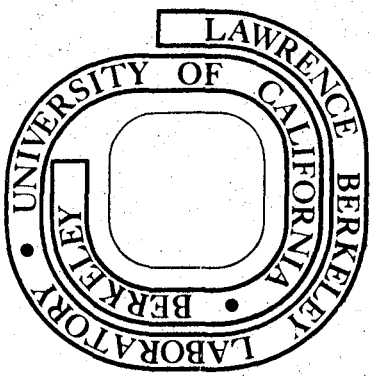

LBL-6612 c.1

LBL-6612

Characterization of Sialon-Type Materials

Paul Newman Spencer
Lawrence Berkeley Laboratory
University of California
Berkeley, California 94720

June 1977

Work performed under the auspices of the U. S.
Energy Research and Development Administration

TABLE OF CONTENTS

I. INTRODUCTION

Concern over finite limitations on energy resources is spurring the search not only for more ways in which to conserve energy but also for ways in which energy can be generated, converted, and stored more efficiently. Particularly pertinent to the need for greater efficiency is the need for better materials. For example, raising the efficiency of gas turbines, by operating them at higher temperatures, could achieve significant results in terms of helping meet future energy requirements and in conserving limited energy resources. This could be done if hot-gas-path components could be fabricated from a material exhibiting the necessary strength and durability at significantly higher operating temperatures and under the associated hot erosion/corrosion conditions. Other examples of more efficient energy conversion systems for which better materials are needed include very large-scale coal gasification plants involving some processes at temperatures up to 3500 °F[1], and fluidized bed applications.

Metals, characteristically ductile, are relatively easily fabricated into complex machinery parts. In addition, they can be alloyed in a reproducible manner to provide very high strength under dynamic and cyclic stresses and resistance to erosion/corrosion at temperatures up to about 1000 °C. For these reasons, over the past two decades the so-called superalloys of metals have filled most needs for high temperature applications other than for refractories. But the superalloys have not been shown to have the potential capabilities to operate and survive in the temperature range (i.e., 1350 °C - 1950 °C) and under the erosion/corrosion conditions now envisaged for many energy-related systems.

Ceramic materials, characteristically brittle, are not easily fabricated into complex shapes. But many of them do have very high melting/decomposition temperatures and relatively high strength at high temperatures. There have not been many attempts in the past at alloying ceramic materials specifically to provide the properties for which the superalloys were created. Because of the apparent temperature limitations on metal alloys, however, a considerable research effort has been devoted in recent years to the development of ceramic materials for superalloy-type applications at the much higher temperature operations needed for greater efficiency in use of fuel.

United States Department of Defense interest, for example, led in 1971 to a 2500 °F ceramic engine research program[2] with Ford Motor Company as the prime contractor and Westinghouse Electric Corporation as the major sub-contractor. Ford is developing a completely ceramic engine for automotive use; Westinghouse is developing first-stage vanes and is establishing guidelines for the use of ceramic materials in large stationary power generation turbines -- both for rotating and static parts. Proponents maintain that ceramic turbines, operating without supplemental cooling, will be 10-30% more efficient than metal turbines while at the same time being able to burn corrosive or low quality fuels which could not be used in metal turbines[3]. This prediction is perhaps optimistic; a review of relevant literature reveals that a number of problems still exist in the attempt to apply basically brittle materials to uses involving cyclic, dynamic stresses, and impact and thermal shock.

Among the various ceramic materials being investigated is silicon nitride and the closely related compound called SIALON, an acronym for

its constituent elements silicon, aluminum, oxygen, and nitrogen. In the last decade, the compound silicon nitride (Si_3N_4) has attracted much attention because of its high decomposition temperature, relatively high strength at high temperatures, good resistance to oxidation and corrosive environments, and relatively good thermal shock resistance. These excellent properties notwithstanding, silicon nitride ceramics have not come into widespread use because of the difficulty in fabricating the material into useable shapes. Satisfactory mechanical properties can only be obtained by hot pressing which process is not economical for mass production. Reaction sintered silicon nitride, while much easier to produce in the shapes required (and thus potentially more economical), has not demonstrated mechanical properties comparable to those of the hot pressed material. In attempting to cope with this problem, researchers have found that metal oxide additives used in preparation of silicon nitride ceramics, either by hot-pressing or by sintering, have resulted in solid solutions that have properties comparable to the hot-pressed pure silicon nitride and are at the same time more amenable to mass production. The first beta-silicon nitride/metal oxide solution was found to exist in the Si_3N_4-Al_2O_3 system by Jack and Wilson[4] in England and simultaneously by Oyama and Kamigaito[5] in Japan. Both reports referred to extensive solid solution formation of Al_2O_3 in beta-Si_3N_4.

There is a considerable difference, however, between producing a material in the laboratory from the pure ingredients and producing it commercially from materials economically available. Thus, other researchers[6,7,8] have been investigating the possibility of producing sialon-type materials by mixing aluminum powder with such abundantly

available materials as volcanic ash or clay, and firing the mixtures in an atmosphere of nitrogen gas.

It is toward investigating this latter possibility that the present work attempted to characterize four different sialon-type materials that were produced in Japan by mixing aluminum powder with volcanic ash and firing preformed billets of the mixture in N_2. A number of mechanical properties were measured as well as the resistance of the materials to oxidation and corrosive atmospheres. An attempt was made to correlate the characteristics with the properties exhibited. Motivating forces for microstructural change under test were monitored. An extensive survey of the literature on the silicon nitrides and sialons was undertaken as a base on which to review and evaluate results. Conclusions were drawn on whether any of the ceramics studied offer possibilities for meeting some of the current needs for high temperature materials.

II. LITERATURE SURVEY

A. Introduction

Because materials bearing the acronym "Sialon" are in a sense synthesized from the silicon nitride structure, a survey of the literature on sialon materials must necessarily start with and contain much on the literature of the silicon nitrides. In the following sections, therefore, available writings on the structures and compositions of the silicon nitrides and sialons, on their properties, and on correlations between the properties and structures of these materials will be reviewed.

B. Structures and Compositions

1. Silicon Nitride. In an extensive review and comment on the literature available up to mid-1973, Croft and Cutler note that although the material had its origins in the nineteenth century (a German patent of 1895 of Mehner), the bulk of the published literature dates from the early 1960's[9]. Particularly with regard to structures and compositions, however, some references prior to that time are of interest.

In early 1957, Vassilou and Wilde reported on heating silicon metal at 1200 °C - 1400 °C in N_2 to get a mixture of two hexagonal forms of silicon nitride. X-ray analysis resulted in their identifying one phase as orthorhombic and the other as hexagonal. For the latter, they approximated lattice parameters of a: 7.60Å and c: 15.70Å[10].

Writing later in 1957, Popper and Ruddlesen reported finding two phases of Si_3N_4, as reported by Vassilou and Wilde, but of structures differing from each other and from the hexagonal reported earlier[11]. They proposed indexing what they termed Phase I as orthorhombic with

parameters a: 3.88, b: 6.71, and c: 5.64Å. Phase II was indexed by them as rhombohedral with parameters a: 8.15Å and α = 108.0°. They did acknowledge a possible hexagonal structure by giving "pseudo-hexagonal" parameters of a: 13.16 and c: 8.72Å; in their opinion this structure was similar to phenacite, Be_2SiO_4. The composition of both forms, they concluded, was "M_3N_4", meaning Si_3N_4.

Hardie and Jack, in August 1957, referred to differences of opinion on structure that had been reported in the literature[12]. They cited the work of Turkdogan, Bills and Tippett (in an article not then published) as having definitely established the existence of two forms of silicon nitride, designated α and β, with the same chemical compositions (Si_3N_4) and the same measured densities (3.19 ± 0.01 gm/ml). Hardie and Jack then reported on their own x-ray examinations which, they maintained, resolved the argument on structure. They reported that α-Si_3N_4 is hexagonal with dimensions of a: 7.608 ± 0.001Å, c: 5.617 ±0.01Å, c/a: 0.7250, and V: 292.0Å^3. On the basis of a unit-cell content of $Si_{12}N_{16}$ for the α form, they calculated a density of 3.184 gm/ml and said this agreed well with the measured density. For β-Si_3N_4, they gave the hexagonal dimensions as a: 7.608 ±0.001Å, c: 2.9107 ±0.0005Å, c/a 0.3826, and V: 145.9Å^3. They calculated a density (in excellent agreement with that they observed) of 3.187 gm/ml based on a unit cell content of Si_6N_8. Hardie and Jack further stated that the structure of β-Si_3N_4 is based on the phenacite type, Be_2SiO_4, in which the oxygen and beryllium atoms are replaced, respectively, by nitrogen and silicon. An irregular tetrahedron of nitrogens is formed with silicon at the center (see Figure 1). Units are joined by sharing corners in such a way that each nitrogen is common to three tetrahedra

as indicated in Figure 2. They report the structure of α-Si_3N_4 as a different arrangement of the same tetrahedral units. Whereas planes of atoms in β are linked along the [001] direction in a sequence ABAB.., they note that the sequence in α is ABCDABCD.....

The materials examined by Hardie and Jack were furnished by Turkdogan, Bills, and Tippett who reported in 1958 on their chemical analysis of silicon nitride prepared by heating pure Si in pure N_2 at 1450 °C[13]. Their original product, which they called "α-Si_3N_4", showed 80 visible diffraction lines in x-ray powder photography. Some of these lines got weaker as the length of nitriding time was increased, and disappeared altogether at a nitriding temperature of 1600 °C. X-ray diffraction of the sample treated at 1600 °C showed only 38 visible lines. Careful analysis, however, showed no change in chemical compositions between this and the original product. They concluded, therefore, that there were two nitrides of silicon: α-, which forms in the presence of elemental silicon, and β-, which forms in its absence. Their report also included the results of Hardie and Jack as covered in the previous paragraph.

The fact that there are two distinct crystallographic forms of silicon nitride, both of apparent composition Si_3N_4, was therefore established by 1958. Figure 3 is a projection of the basal plane of α- and β- silicon nitride as depicted by Thompson and Pratt[14]. They note that the large void formed by the hexagonal arrangement is continuous through the beta lattice, but that in the alpha structure the basal plane is alternated with a mirror image of itself and thus the continuous void of the beta structure becomes in the alpha a series of pockets. They state that large atoms (1.5Å radius) could diffuse

readily through the beta lattice while the alpha lattice would tend to trap atoms of such radii. The channels in the alpha structure (between the "pockets") through which atoms could diffuse would allow a sphere of only 0.7Å to pass.

Five years later, Wild, Grieveson, and Jack observed that the relationship between the two forms of silicon nitride, α and β, remained obscure. They reported on their determination of the crystal structure of α-silicon nitride and on further refinement of the parameters of the β-silicon nitride structure[15]. Their point of departure, essentially, was that both the α and β forms are hexagonal with the c dimension of α being approximately twice that of β with the suggested layer sequence for α being ABCDABCD... and that of β being ABAB... Their determination of unit cell dimensions was from x-ray powder photographs. The β structure they defined as consisting of SiN_4 tetrahedra joined by sharing nitrogen corners so that each nitrogen is common to three tetrahedra (see Figure 4). For the α structure, they established a unit cell containing sites for twenty-eight atoms, $Si_{12}N_{16}$, divided into four different type nitrogen sites: N1, N2, N3, and N4; and two different type silicon atom sites: Si1 and Si2 (see Figure 5). The x-ray studies showed that the N1 sites cannot always be occupied solely by nitrogen and must contain a proportion of atoms of higher atomic number, most likely oxygen. They postulated a defect structure with about 25% nitrogen vacancies in site N4, a partial replacement of nitrogen by oxygen in site N1, and an appropriate number of silicon site vacancies to maintain electrical neutrality. This results in a much greater distortion of the MN_4 tetrahedra for the α structure than is the case in the β structure. They conclude that their work has

established α - silicon nitride as an oxynitride.

2. Sialon. Knowledge of the existence of solid solutions of certain metal oxides in silicon nitride appeared at the beginning of the 1970's. Oyama and Kamigaito, in 1971, mixed powdered Si_3N_4 with alpha-alumina and/or lithium carbonate and hot pressed the mixture under 300 kg/cm^2 pressure at 1750 °C for 20 minutes. X-ray diffraction patterns of the resulting material showed not only Si_3N_4 but a new phase as well. The new phase unexpectedly produced x-ray diffraction lines almost identical to those of pure β-Si_3N_4 but in each case shifted to a lower diffraction angle. The shift was reported to be nearly proportional to the content of the metal oxide added. Oyama and Kamigaito concluded that the new phase was a solid solution of Si_3N_4 - Al_2O_3 or Si_3N_4 - Li_2O[16].

In January 1972, Oyama made reference to his and Kamigaito's previous work and stated that the solid solution in Si_3N_4 - Al_2O_3 was considered to be of a substituional type based on specific gravity measurements[17]. He considered that some vacancies in Si sites must be present in order to satisfy charge neutralization, assumed that AlN constitutes a substitutional solid solution in the Si_3N_4 - AlN-Al_2O_3 system, and concluded that some of the vacancies must be annihilated in proportion to the AlN concentration. This, he considered would give higher stability to the solid solution. When the AlN molar concentration is equal to that of Al_2O_3, the solid solution was thought to have the lowest vacancy density and, hence, be most stable. He argued that the solubility limit of AlN depends on the vacancy density in the N-sites, because the sp^3 silicon atomic orbital combines with the sp^2 nitrogen atomic orbital and an N-vacancy modified the Si sp^3 orbitals

destructively giving a high energy of formation for the N-vacancy. Thus, he noted that the solubility of AlN in Si_3N_4 could hardly exceed the concentration of Al_2O_3 in solid solution because N-vacancies would need to be formed. He presented the approximate phase diagram shown in Figure 6 and postulated a region of solid solubility for the Si_3N_4 - Al_2O_3 - AlN system. He supported this theoretical argument with reports on the x-ray diffraction analysis of the product formed from sintering a mixture of Si_3N_4, Al_2O_3, and AlN powders in a graphite die under 250 kg/cm^2 pressure for 30 minutes at 1730 °C. The results show a new phase closely resembling Si_3N_4, which he considers to be a solid solution, Si_3N_4 - Al_2O_3 - AlN with observed solubility limits very close to that postulated in his suggested phase diagram (see Figure 6).

Later, in 1972, Jack and Wilson reported on a variety of ceramic materials built up of $(Si,Al)(N,O)_4$ units[18]. They hot pressed mixtures of α - silicon nitride and alumina at 1700 °C for one hour and analyzed the results by x-ray diffraction. They indexed the reflections on the basis of an expanded hexagonal β-Si_3N_4 structure, which they now called β^1. They presented results showing that the unit cell dimensions increased according to increasing alumina content: cell dimension a increasing from 7.61Å at zero w/o alumina to nearly 7.72Å at 90 w/o alumina; cell dimension c increasing from 2.91Å at zero w/o alumina to about 3.00Å at 90 w/o alumina. Considering a β^1 unit cell of eight atoms of nitrogen and oxygen (e.g., β-Si_6N_8), they noted a range of homogeneity $Si_6N_8 \rightarrow Si_{(6-0.75x)}Al_{0.67x}N_{(8-x)}O_x \rightarrow Al_{5.33}O_8$ where x, the number of nitrogen atoms in the cell replaced by oxygen, varies from 0 to at least 5. Postulating that for each nitrogen atom replaced by oxygen, three-quarters of a silicon is replaced by two-thirds of an aluminum

atom -- in order to maintain electrical neutrality, they note excellent agreement between calculated values and observed analysis for silicon, aluminum, oxygen, and nitrogen. The use of the symbols Si, Al, O, and N in the title of their report may have been the genesis for the acronym "sialon".

In Japan, in early 1975, Umebayashi and Kobayashi, aware of the work of previous researchers on sialon, undertook an attempt to form sialon-type materials by mixing volcanic ash with various amounts of aluminum powder, preforming the mixture under pressure, and heating the preformed billets at 1400 °C for 5 hours in N_2[19]. For 20 w/o Al powder in the mix, x-ray diffraction revealed a product consisting of Si, α-Al_2O_3, and a small amount of β-Si_3N_4. As the Al powder content in the mix was increased, the Si diffraction peak disappeared and the β-Si_3N_4 peak intensity increased; the intensity of the α-Al_2O_3 peak increased slightly for Al contents up to 35%, decreased gradually up to 40% Al, and decreased rapidly above 50% Al. An unknown phase appeared in the 35% to 50% Al range with the peak intensity increasing proportionally to the increasing Al content in the starting mix. These researchers observed β-Si_3N_4 peak shifts almost identical to the shifts reported by Jack and Wilson.

Reporting later in 1975, Umebayashi and Kobayashi discussed the results obtained when they used a starting mixture of volcanic ash and 40 w/o Al powder, preformed it under 400 kg/cm^2 pressure, and heated the billets in an N_2 atmosphere at various temperatures (1100-1400 °C) and at various holding times at temperature (0 to 10 hours)[20]. X-ray diffraction showed Si, α-Al_2O_3, and AlN present after the 1100 °C treatment. With increasing temperature, the Si was suggested to have

converted to a β-Si_3N_4 form exhibiting lower diffraction angles than pure β-Si_3N_4. The AlN observed after 1100 °C treatment was not in evidence in diffraction peaks taken after the 1300 °C treatment, while the β-Si_3N_4 peaks had increased substantially. The simultaneous disappearance of AlN and increased presence of β-Si_3N_4 indicated to Umebayashi and Kobayashi a solution of AlN in β-Si_3N_4. They noted that their β-Si_3N_4 product was almost identical to the β-Si_3N_4-Al_2O_3-AlN solid solution reported by Oyama[17] and concluded that the components dissolved in their β-Si_3N_4 were AlN and Al_2O_3.

Still later in 1975, Gauckler, Lukas, and Petzow reported on their contribution to the Si_3N_4-AlN-Al_2O_3 phase diagram of the system Si-Al-O-N[21]. They represented this system as a square plane subsection contained in a tetrahedron (see Figure 7). The 1760 °C isothermal section of this plane, showing phase equilibria in a quasi-ternary section is reproduced at Figure 8. They assume that the valances (Si^{4+}, Al^{3+}, O^{2-}, N^{3-}) do not change and thus that all phases existing in equilibrium will be in this plane. They refer to phase X_1 (see Figure 8) as that reported previously (by Oyama and Kamigaito in 1972 and by Jack in 1973) to have a composition on SiO_2-AlN, but added that their work showed that X_1 should lie closer to mullite in the phase diagram. Citing their x-ray diffraction work, they maintain that the β^1 region is narrower than that previously postulated in the literature. Their results show the β^1 region to extend in the Si_3N_4-AlN-Al_2O_3 direction. This line represents a constant cation/anion ratio of 3:4 and the β^1 phase can therefore be described by the empirical formula $Si_{6-x}Al_xO_xN_{8-x}$, with x equal to 0-4.2. They explain the difference in width of their β^1 region from widths previously reported as probably

due to different starting mixtures. Single phase β' specimens can be obtained, they say, by sintering mixtures lying on the Si_3N_4-Al_2O_3 diagonal at temperatures about 1800 °C. With increasing AlN concentration, five new phases (X_2, X_4, X_5, X_6, and X_7 in Figure 8) were identified by x-ray diffraction. As noted, the phases cover narrow, elongated single-phase regions oriented along lines of constant cation/anion ratios.

Shortly after their contribution to the sialon phase diagram, Gauckler and Lukas published another paper on β-Si_3N_4 solid solutions containing metal oxides[22]. Noting that the solid solubility limits of different metal oxides in β-Si_3N_4 depends on the size and charge of the metal elements, they proposed a misfit factor as a means of considering numerically the variables of solubility. They found that a substantial amount of foreign atoms could be accommodated in the β-Si_3N_4 lattice when their misfit factor was small. When the misfit factor calculation resulted in a large value, they found that only a few foreign atoms would enter the lattice. They suggested, therefore, that their misfit factor could be used to estimate the solid solubility limits of one or more metal oxides and nitrides in β-Si_3N_4. The existence of other factors strongly affecting solid solubility (such as the fact that the nature of the chemical bonds in the β-Si_3N_4-metal oxide solid solutions are unknown) was cited in summary as a basis for using the misfit factor with caution.

Most recently, Lewis, et at, have published a paper reporting on microstructural analysis by transmission electron microscopy and Auger electron spectroscopy of what are essentially single-phase Si-Al-O-N ceramics prepared by hot-pressing mixtures of Si_3N_4, AlN, and SiO_2 (with

additives of 1% MgO) having varying ratios of AlN/SiO_2[23]. They examine the densification process as it is affected by different starting compositions. They report that the presence of the 1% MgO additive was shown to accelerate densification by forming a low melting point silicate (through reaction with SiO_2) and thus assisting the early solution of AlN and the reprecipitation of β' substituted crystals. When the starting composition was near that represented by the so-called "z" formula, i.e., $Si_{6-z}Al_zO_zN_{8-z}$, their transmission electron microscopy revealed, however, a difference in grain morphology and absence of a residual glassy phase. In this material, they note much larger β' grains, possibly explained by the absence of the inhibiting effect of a residual glassy phase on grain growth. They conclude, in this connection, that for the materials with a residual glassy phase, grain boundary migration requires the solution and reprecipitation of β' components in order for the diffusional transfer of atoms across the boundary (i.e., grain boundary migration) to take place. From their analysis of microstructure by transmission electron microscopy and Auger electron spectroscopy they present a three-stage densification mechanism: (i) initial liquid formation facilitating particle rearrangement; (ii) dissolution of AlN and formation of x-phase liquid plus β'-Si_3N_4; and (iii) dissolution of Si_3N_4 (both α and β) and reprecipitation of more β' solid solution with simultaneous removal of porosity. They report that MgO presence in small amounts enhances the reactions in (i) and (ii) but that it does not appear to increase the rate of either phase transformations or densification in stage (iii).

The presence of an intergranular glassy second phase in a MgO hot-pressed silicon nitride has been verified by Clark and Thomas[24].

From high resolution electron microscopy lattice imaging studies they conclude that while the intergranular phases do indeed exist they are heterogeneously distributed especially appearing at multiple grain junctions.

It may be concluded from this portion of the literature survey that a great deal has been learned in recent years about the structures and compositions of the silicon nitrides and the derivative sialons. Most interest now seems to center on quantifying the structural and compositional phenomena involved in the "alloying" of β silicon nitride with various metal oxides.

C. Properties

1. Silicon Nitride. The engineering interest in silicon nitride derives from its oft-quoted properties of high strength, good wear resistance, high decomposition temperature, oxidation resistance, excellent thermal-shock properties, low coefficient of friction, and resistance to corrosive environments[25]. A summary of some of these properties has been prepared by Croft and Cutler and is reproduced at Table 1[26].

According to information published by the Metals and Ceramic Information Center, silicon nitride does not melt, but decomposes at approximately 1871 °C in nitrogen by the reaction $Si_3N_4 \rightarrow 3Si + 2N_2$[27]. Thermal conductivity for hot-pressed silicon nitride is reported by George to range from about 30 W/m/°K at 700 °K to about 20 W/m/°K at or near the decomposition temperature, and for reaction-sintered Si_3N_4 to remain in the vicinity of 5 W/m/°K throughout the same temperature range[28]. George notes that the conductivity is quite sensitive to density, but that there is no correlation between density and

conductivity, indicating that phase composition is important. He notes that the presence of a free silicon phase, for example, is "beneficial" because its conductivity is higher than that of the other phases.

Torti, et al, report the thermal conductivity of hot pressed and reaction-bonded Si_3N_4, respectively, as 30 W/m/°K (18 BTU/hr/ft/°F) and 14 W/m/°K (8 BTU/hr/ft/°F)[29]. They also report a coefficient of thermal expansion, in the temperature range 20-1500 °C, of 3.2×10^{-6}/°C for both hot-pressed and reaction-bonded Si_3N_4.

The strength of reaction-bonded Si_3N_4 ceramics is discussed by Godfrey and Lindley as extending up to 45×10^3 psi[30]. They investigated the effect on strength of different firing schedules, differences in starting mixtures, and particularly differences in the number and size of voids. One surprising finding was their report that weak material exhibited less visible voids in photomicrographs than did strong material. Further study showed, however, that large voids in the region of maximum stress weakened the material considerably. They found circumstantial evidence that contamination of furnace atmospheres may reduce strengths up to 25%.

Reporting on mechanical properties of silicon nitride at elevated temperatures, Ashcroft compared the modulus of rupture of commercial varieties of hot-pressed and flame-sprayed material[31]. He found the former about four times stronger at low temperatures but above 1400 °C found both materials of similar strength. He maintained that hot-pressed silicon nitride is not completely brittle at high temperatures and shows some plasticity during loading at 1200 °C and above. He noted also a delayed fracture phenomenon in hot-pressed silicon nitride under constant stress, occurring at about 60% of the bend rupture modulus at

900 °C and at about 85% of the bend rupture modulus at 600 °C. He suggested that oxidation is not the primary cause of strength reduction at high temperatures, but that an oxidized layer would have a deleterious effect if the temperature were cycled.

Noakes and Pratt investigated the dependence of the modulus of rupture and the modulus of elasticity on the isostatic pressing pressure for reaction-sintered Si_3N_4[32]. They also made microhardness tests on the α and β phases. Their results showed that pressing pressures did not significantly effect the materials at testing temperatures below 800 °C but that there is a significant increase in the modulus of rupture between 1000 °C and 1200 °C probably due to the onset of plasticity. They found that the modulus of elasticity increases significantly with higher pressing pressures; this results in a range of 82 - 135 MN/m^2 for a porosity range of 19 - 23%. They suggested granular sliding as an important deformation mechanism above 1000 °C and noted agreement with other reports that the α:β ratio has little effect on the modulus of elasticity.

Relating structure to bulk mechanical properties, Coe, Lumby, and Pawson undertook extensive microhardness testing[33]. Of interest in their report is their statement that consistent microhardness values were obtained only when specimens were prepared on a lap using 0.3 micron diamond powder, and that this is, significantly, similar to the average grain size. From their micro-hardness testing, they conclude that hardness is inversely proportional to grain size and strength.

Petrovic, et al, used Knoop microhardness indentations to introduce controlled surface flaws in hot-pressed silicon nitride[34]. Noting that a microhardness indentation on the tensile surface of a

bend specimen initiates fracture because it is the worst flaw in the specimen, they used such controlled flaws to obtain K_{1C} values at both ambient and high temperatures. Their results showed that use of controlled flaws reduces the magnitude and scatter of room-temperature fracture strengths while at the same time facilitating the attainment of K_{1C} values consistent with those obtained by other more difficult means. They conclude that their method is attractive for its simplicity and because the cracks produced closely approximate actual failure defects in ceramics. Their K_{1C} results (for NC-132 Si_3N_4) fell in a range of from 4.2 to about 4.7 $MN/m^{3/2}$.

Not too much is reported in the literature on the steady state creep of silicon nitride. One published article, by Ud Din and Nicholson, discusses the creep deformation of reaction-sintered silicon nitrides[35]. They loaded specimens in 4-point bending at stresses ranging from 10,000 to 20,000 psi at temperatures from 1200 °C to 1450 °C. They found that the creep rates were proportional to the 1.4 power of the stress. A creep activation energy of 130 ± 5Kcal/mol was determined. Their transmission and scanning electron microscopy investigation of creep specimens led them to suggest that the rate-controlling mechanism of creep is grain-boundary sliding.

Because silicon nitride is a candidate material for gas turbine engines, Ammann, et al, used slow crack growth data to predict the thermal fatigue life of silicon nitride parts subject to cyclic thermal stress[36]. They devised a computer program for numerically calculating the extent of slow crack growth for successive thermal cycles until catastrophic failure. Their results led them to suggest that silicon nitride can be made more resistant to thermal fatigue by minimizing

the amount of viscous grain-boundary phase, which, they say, is responsible for slow crack growth.

Also writing on high-temperature thermal fatigue, Hasselman and Chen investigated the role of activation energy (Q) for slow crack growth[37]. They found a value for Q of 160 Kcal/mol. They suggested that activation energy plays a more important role than the stress exponent (n) in determining fatigue life (i.e., $V = Ak^n \exp(-Q/RT)$ where A and n are constants, R is the gas constant, and T is temperature).

The work of Barnaby and Taylor on the fracture resistance of silicon nitride is of interest because they describe use of testing techniques applicable to high-strength metals to achieve reproducible and accurate measurements of the fracture toughness of silicon nitride[38]. This toughness, they conclude, is dependent on the relative content of pores, α and β phases, and possibly on the content of residual silicon. Toughness, as they determined it, shows a trend to higher values for predominantly α structures and decreases, as may be expected, with an increase in fractional porosity.

Writing on the oxidation of silicon nitride powder, Horton proposed the oxidation reaction $Si_3N_4 + 3O_2 \rightarrow 3SiO_2 + 2N_2$ and noted that the weight gained represents the weight difference between Si_3N_4 and SiO_2[39]. He found that complete oxidation of a sample causes a weight increase of over 28%. His study of oxidation led him to suggest that the rate of oxidation is diffusion controlled.

Kiehle, et al, have investigated the oxidation behavior of hot-pressed Si_3N_4[40]. They found that a distinct amorphous film is produced on Si_3N_4 surfaces heated for 24 hours at 750 °C and that as the

heating time or temperature increases, this amorphous film devitrifies to cristobalite particles. They found also that at temperatures above 1000 °C, SiO_2 reacts with impurities to form acicular silicate crystals indentified by x-ray diffraction as enstatite, forsterite, akermanite, and diopside. They note that porosity develops as gaseous reaction products erupt from beneath the reacted layer. They conclude that additives (introduced for better mechanical properties) greatly lower the oxidation resistance of Si_3N_4 and that the upper limit for which Si_3N_4 remains chemically stable in air is about 700 °C.

Singhal reports that water vapor enhances the oxidation rate of silicon nitride[41]. He finds it difficult, however, to differentiate the effects of impurities (such as Ca, Mg, Na, K, etc.) which may be present in the hot-pressed Si_3N_4, from the effect of the water vapor.

In the area of erosion/corrosion resistance, Rowcliffe and Huber have written on hot gas corrosion of silicon nitride[42]. They refer to previous reports which indicate that the corrosion resistance of silicon nitride is very good but that a combined erosion-corrosion effect was noted in simulated turbine environments. Their experiments showed that slow crack growth can be considerably influenced by environment. For two different commercial Si_3N_4 materials, they found that failure times were considerably reduced in flowing hot gas. The principal effect, they say, is one of corrosion since localized attack was observed at the roots of notches. They believe that small additions of elements such as sodium, magnesium, and vanadium do not affect crack growth. In some instances, they report, corrosion leads to an increase in apparent toughness at low temperatures, probably because of changes in the shape of crack tips.

2. Sialons. Although many general statements attesting to the excellent properties of sialon have been made in the literature, until recently there has been a dearth of specific information. This is illustrated by Table 2 which lists the same properties as for silicon nitride (shown in Table 1) but shows a number of them not readily available in the literature as of January 1977.

A handbook on ceramic properties, issued by the Metals and Ceramics Information Center summarizes sialon properties briefly[43]. Their thermal decomposition is said to be similar to that for Si_3N_4 and a generalized working temperature of 1760 °C is listed. This reference notes that as of March 1976, no information was available in the literature on specific heat or thermal conductivity. No information is reported on the modulus of elasticity or on microhardness. Other properties such as thermal shock and oxidation resistance are reportedly comparable to Si_3N_4 properties.

In their original paper specifically on sialon (i.e., β'-Si_3N_4), Jack and Wilson give some specifics[44]. They list the linear coefficient of thermal expansion to be 2.7×10^{-6}/°C as determined by x-ray methods and 3.0×10^{-6}/°C as determined by dilatometric means. They reported excellent thermal shock properties as determined from repeatedly dropping fabricated shapes into cold water from 1200 °C without cracking. The preliminary modulus of rupture at room temperature was reported by Jack and Wilson to exceed 40,000 psi. As perhaps the most advantageous property of sialon, Jack and Wilson list ease of fabrication, noting that sialon can be sintered to maximum density in an inert atmosphere at about 1700 °C.

Reporting on pressure sintering of sialon, Yeh, et al, stated that

pore free bodies were obtained at temperatures as low as 1500 °C for the 40 Si_3N_4 - 60 Al_2O_3 (mol %) composition and that fully dense bodies could be obtained at 1200 °C at 4000 psi with no holding time[45]. Early in 1977, Wills, et al, reported on the effect of composition and x-phase on the intrinsic properties of reaction-sintered sialon[46]. They concluded that densification is enhanced by reducing the Si_3N_4 content of the Si_3N_4-Al_2O_3-AlN mix. Also, they reported finding that the thermal properties of sialon can be considered invariant with composition. Their evaluation of the x-phase is that it is detrimental to fracture toughness properties. In a concurrently published paper, Wills, et al, reported a room temperature bend strength of 51,000 psi[47]. They noted that strength degradation occurred as a result of subcritical crack growth activated by grain boundary sliding. Table 3 is adapted from their recent listing of the intrinsic properties of sialon. Table 3 supplements the information given in Table 2.

Lumby, North, and Taylor investigated the chemistry of sialon with specific reference to creep[48]. They varied the amount of AlN in mixtures of Si_3N_4, AlN, SiO_2, and MgO and measured the creep rate for the different mixes. Their report shows that, as AlN content is increased, creep after 20 hours at load decreased from 0.275% strain for a mix with less AlN down to 0.006% strain for a mix with an extra 3 1/2% AlN. This demonstrates, they conclude, a determination of some measure of control of the glassy phase in some sialon compositions. This finding is correlated with later work reported in another publication previously mentioned in which the authors teamed with Lewis, Powell, and Drew[49]. In this later work, it is concluded that the best compromise between ease of processing and good high temperature properties is likely to

be achieved with additives which promote crystallization of the glassy phase, thus eliminating the more rapid viscous flow mechanisms for creep and delayed fracture.

Jack and Wilson reported on the oxidation of β^1-Si_3N_4[50]. They oxidized in air at 1200 °C a small specimen and found a weight loss of 0.04% after 30 minutes but no weight loss after 6 hours more at that temperature. They attributed the 0.04% loss to volatilization of surface moisture.

In a recent report, Schlichting and Gauckler listed results from oxidizing a variety of sialon-type materials, i.e., β-Si_3N_4 with various metal oxides added[51]. For all specimens a parabolic weight increase was observed.

β^1-Si_3N_4 sialon specimens, however, showed a lower rate of oxidation than did the sialons containing Al_2O_3 and MgO. They attribute this to the formation on the β^1-Si_3N_4 surfaces of crystalline cristobalite or mullite phases with low oxygen diffusivity. Oxygen cannot penetrate the crystals but must move along the crystal grain boundaries. Thus the area vulnerable to oxidation is reduced.

Lee, Cassarini, and Cutler report on properties of sialons derived from clay[52]. They state that (clay) sialons compare favorably with other refractories in regard to all the important factors: high melting temperature, low thermal expansion, high temperature strength, good sintering properties, no phase transformations, and resistance to oxidation.

D. Correlation Between Properties and Structures

1. Silicon Nitride. Lange raised the obvious question, in discussing structure and properties, of what is the effect on strength

of secondary phases observed in the microstructure[53]. He studied relationships between properties and microstructures primarily from the standpoint of inclusions as crack precursors and reported that no strength degradation is observed when the size of the inclusion (secondary phase region) is approximately the same as the grain size of the matrix. He discussed two models which suggest how a liquid phase may influence mechanical properties: one in which the liquid phase enhances creep by providing regions or paths of high diffusion conductance; and another (his) which considers that grain boundary sliding and separation are the primary mechanisms of non-elastic deformation. He cites experimental evidence which strongly suggested that the liquid phase was the dominant microstructural feature of deformation by grain boundary separation and sliding. Lange refers to the fibrous grain morphology of hot-pressed Si_3N_4 and cites x-ray experiments that showed preferential alignment of fiber axes perpendicular to the hot-pressing direction. Subsequent flexural strength measurements, he noted, showed that specimens cut and stressed perpendicular to the hot-pressing direction were 20% stronger than specimens cut and stressed parallel to the hot-pressing direction. He suggests that the effect of impurities (or additives) on fabrication, microstructure and properties can best be approached through phase-equilibrium studies. It should be noted, that, given the right additives, a sialon would result and Lange's suggestion on strength versus pressing direction would thus apply to the sialon.

In an earlier report, Lange reported on scanning electron microscope examination of fracture surfaces[54]. The reason for the high fracture energy of strong Si_3N_4, he reported, appeared to be its grain morphology. Materials having the highest fracture energy had an

elongated grain structure and a rough fracture surface that contained many holes.

In still another report on Si_3N_4, Lange and Iskoe included some excellent scanning electron microscope photographs which would be useful for others researching Si_3N_4[55].

Relating effects of oxidation on the strength of reaction-sintered silicon nitride, Davidge, et al, used measurements of weight gain as well as x-ray diffraction and microscopy on specimens which had been oxidized in air at temperatures from 1000 °C to 1400 °C[56]. The major oxidation product, they found, was cristobalite, with the weight gain being proportional to $(\text{time})^{1/2}$. Scanning electron microscopy on the polished surfaces of unoxidized specimens showed flat polished plateaux and a porous background, while the oxidized specimens, for short times at a temperature of 1200 °C, revealed a relatively smooth dense surface layer. The oxide layer, after heating at 1400 °C, was severely cracked showing a grid of wide cracks about 100 microns apart and an intermediate network of narrow cracks about 20 microns apart. They noted that the thickness of the surface layer increased with increased oxidation time. From their observations of the different microstructures of specimens oxidized at 1000 °C, 1200 °C, and 1400 °C, they suggested that the oxide must have a relatively low viscosity at the higher temperatures because it apparently runs into pores to generate flat surfaces at those temperatures. In an earlier paper, Evans and Davidge had made the observation that in cristobalite-producing oxidation less than 1/4 of the total cristobalite is in the surface layer[57]. They presumed that the bulk of the oxidation had occurred throughout the specimen, probably around the pores.

Also concerned with the effect of oxidation on strength, de S. Jayatilaka and Leake used scanning and transmission electron microscopy in an attempt to learn more of the correlation of microstructure to such properties of reaction-sintered silicon nitride as Young's modulus and the modulus of rupture (they noted the limited usefulness of optical microscopy because of the very fine-grained nature of the material)[58]. In particular, their micrographs showed bright rings in each pore of specimens heated at temperature below 1000 °C. That these rings are due to the presence of amorphous silica, they report as confirming earlier suggestions by others. They also observed large unreacted silica particles on a fracture surface and suggested that such particles may initiate fracture at lower than expected stresses. They concluded that much is yet to be learned about detailed microstructural changes due to oxidation but that the formation of thin layers of amorphous silica in pores within the material is certainly important.

Dalgleish and Pratt used optical and scanning electron microscopy to study pore size as a function of nitriding conditions as it affects strength properties[59]. They concluded that the strength of reaction-sintered silicon nitride is determined by the size of the largest pore present. Increased fracture strength was mainly associated, they say, with reduced silicon particle size.

The role of impurities containing Fe and Al in the formation of Si_3N_4 by reaction bonding silicon powder was assessed by Godfrey[60]. His microstructural observations revealed an unusual absence of large voids. This absence, he speculated, was due to an impurity-facilitated diffusion mechanism. He concluded that his findings lent support to suggestions that β-Si_3N_4 is dependent on the presence of impurities for

its existence (and properties).

Reporting on a study that compared microstructural observations to fracture strength, Coppola, et al, made these points: (1) all hot-pressed silicon nitrides appear to have uniform grain sizes with little or no porosity, while the reaction sintered materials exhibit considerable porosity separating needle-like grains; (2) fractographs of hot-pressed specimens showed extensive surface flow at 1200 °C and indications of surface flow at 800 °C; (3) both hot-pressed reaction-sintered materials showed the same general temperature variation, i.e., a low temperature region of decreasing fracture surface energy with increasing temperature followed by a high temperature region of rapidly increasing fracture surface energy; (4) the rapid increase in fracture surface energy was attributed to the extensive flow observed in the microstructure; and (5) the observed fracture behavior suggests that in the hot-pressed material the elevated temperature flow is a combination of both dislocation plastic flow mechanisms and viscous flow of the additive glassy phase, while in the reaction sintered material the flow is only the dislocation plastic flow mechanism[61].

2. Sialon. As emphasized earlier in the literature survey, a separate treatment of sialon is somewhat arbitrary because the sialons are "built up" by adding to, but not changing except in unit cell dimension, the basic silicon nitride structure. Thus, correlations of microstructure and properties for silicon nitride apply at least in part to sialon, and vice versa. Also, as stated earlier, the literature on sialon is still relatively sparse. A recent paper by Seltzer is of interest, however, in comparing microstructures of sialons to strength properties[62]. He studied creep mechanisms operative under various

conditions of stress and environment. He used optical metallography to reveal general microstructural features and scanning and replica electron microscopy to determine grain size and distribution of porosity on grain boundaries of fractured specimens. He noted that the sialons appear to have equiaxed coarse grained structures as compared to Si_3N_4 materials and that the major crystalline phase in each sialon composition was the expanded β-$Si_3N_4(Al_2O_3)$ solid solution. Comparing his microstructural observations and measurements, he concluded that the grain boundary sliding mechanism that controls creep in hot-pressed Si_3N_4 is operative also for some sialon materials. He adds, however, that sialons with low Al_2O_3 concentration appear to have different creep mechanisms, the predominant mode of which appears to involve viscous creep controlled by self-diffusion.

3. Effect of microstructure on rate of machining. Rice and Speronello have studied the effect of microstructure on the rate of machining of ceramics[63]. Their subject is pertinent to the correlation of microstructure and properties in the present work. Proceeding from the postulate that the size of flaws left in the surface by machining is directly related to machining forces, they found that machining difficulty increased with decreasing porosity and grain size. For materials with non-uniform distributions of grain size or porosity, they report machining rates as being controlled by the smaller grains and least porous regions. They suggest that machining difficulty is directly proportional to hardness and compressive strength.

III. EXPERIMENTAL PROCEDURES

A. The Material

Four different sialon-type materials were received from K. Kobayashi of the National Industrial Research Institute of Kyushu, Japan. The materials were prepared from a starting mix (in varying mixing ratios) of Shirasu volcanic ash plus aluminum powder (and/or silicon powder), preformed under pressure, then sintered or hot-pressed in a nitrogen atmosphere at various temperatures in the 1400 °C to 1700 °C range. The Shirasu volcanic ash, abundantly available on Kyushu Island in Japan, has a chemical composition range of: SiO_2 - 65-73%; Al_2O_3 - 12-16%: FeO plus Fe_2O_3 - 1-3%; CaO - 2-4%; MgO - less than 1.5%; Na_2O - 3-4%; and K_2O - 2-4%. For the preparation of the sialons, the fraction of the ash with specific gravity greater than 2.4 was used. The chemical composition of this fraction in w/o was reported to be: SiO_2 - 63.7; Al_2O_3 - 19.6; FeO plus Fe_2O_3 - 3.8; CaO - 5.4; MgO - 1.2; Na_2O - 5.0; K_2O - 1.0; with loss on ignition of 0.5 w/o. The aluminum powder used was reported as -100 mesh, purity 99.7%[6,7]. For testing purposes, the materials received were identified as M1, M2, M3, and M4; they are further described as follows:

1. M1. Prepared from a mixed powder of Shirasu volcanic ash and aluminum powder (reported mixing ratio of 60:40). The mix was preformed under a pressure of 400 kg/cm^2 and heated in N_2 for 5 hours at 1400 °C.

2. M2. Prepared from a mixed powder of Shirasu volcanic ash and aluminum powder (reported mixing ratio of 40:60). The mix was preformed under a pressure of 400 kg/cm^2, heated in N_2 for 5 hours at 1400 °C, crushed and ground, then hot-pressed at 1700 °C using a

graphite die under 200 kg/cm^2 pressure.

3. M3 and M4. Prepared from volcanic ash, aluminum powder, and silicon powder (mixing ratio of 60:40:40), preformed under a pressure of 400 kg/cm^2, crushed and ground, then hot-pressed at 1700 °C using a graphite die under 200 kg/cm^2 pressure. These specimens of similar composition apparently were made at different times.

B. Characterization Methods

Data on Si_3N_4 and sialon-type materials were assembled from the literature. These data include crystal structures, chemical compositions, x-ray analyses, optical and scanning electron microscope observations of microstructures, and mechanical, thermal, and oxidation and corrosion resistance properties. As much similar data as could be produced by experiment in the time available were then obtained. Comparisons of these data are presented and discussed in the Results and Discussion section. Mechanical tests included compressive tests at temperatures ranging from 1200 °C - 1500 °C, room temperature 4-point bend tests -- some after thermal shocking of specimens, and determinations of the microhardness of the different specimens both before and after the compressive testing.

C. Specimen Preparation

Only one sample of the M1 material was received. This was a rectangular shapes billet measuring 50 x 25 x 5 mm. Two cylindrical billets, approximately 25 mm in diameter and 5 mm thick, were received of materials M2, M3, and M4. These billets were cut to specimen size on a high-precision, 19,000 rpm grinder using a 0.010-in. D220 grit MA 1/16-in. diamond slicing blade. Because the grinder enabled depths of cut to 0.0005 in., the depth of cut that could be accommodated, at

a steady rate of table movement without obvious overstress on the blade, was used as an estimated measure of machineability. After slicing, specimens were hand ground to size using silicon carbide papers, and 120- and 220-grit diamond wheels. Corners were slightly rounded on 240-grit SiC paper to remove chips.

D. Mechanical Testing

1. Compression Tests. Specimens of each material 0.3-in. in length and 0.1 in. x 0.1 in. in cross section, cut with long axis perpendicular to the pressing direction, were subjected to compression at temperatures ranging from 1200-1400 °C; one sample was tested at 1500 °C. An Instron testing machine was fitted with alumina rams passing into a locally fabricated, resistance type furnace. The specimen was placed between SiC spacers as shown in Figure 9. A crosshead speed of 0.0002 in./min was used in all of the tests. During the heat up to test temperature, a stress of approximately 1000 psi was maintained on the specimen. A temperature stabilizing period of one hour was used. Load versus time readings, which could be converted directly to stress-strain measurements, were recorded.

2. Bend Tests. The same test assembly as for the compressive tests, with a steel 4-point jig being placed between the alumina rams, was used for the room temperature bend tests. Two different geometrical configurations were used for the bend test specimens: 1.2 in. in length, 0.2 in. in width, and 0.08 in. in height for one configuration, and 1.2 in. in length, 0.1 in. in width, and 0.1 in. in height for the other. The arrangement of the specimen and jig are shown in Figure 10. A number of the room temperature bend tests were made after the specimens had been thermally shocked. Alumina specimens of the same two configurations

were also tested in order to determine at least qualitatively, whether different configurations yield different results generally in the bend testing of ceramic materials.

3. Thermal Shock Tests. Specimens were placed in a platinum crucible and suspended on platinum wire in a resistance furnace at 400 °C for 15 minutes. The crucible was then released to drop into water at room temperature.

4. Microhardness Testing. A Leitz microhardness tester was used with 400X magnification being required in order to observe the very small diamond indentations in the variegated microstructure after polishing and light etching. A 1000 gram load was used in all cases for a standard cross-reference.

E. Other Properties Investigated

1. Densities. The Archimedes principle, with distilled water as a medium, was used for density and percent open porosity measurements. Both polished and as-cut samples were used to determine whether polishing produced significant differences in results.

2. Oxidation/Corrosion. An indication of how the materials were affected by oxidizing conditions was obtained during the compressive testing. Specimens were laid in the furnace, on the lower SiC spacer, next to those being compressed. Oxidation was estimated by weight gain and by microscopic observation of changes in the surface. Also, x-ray diffraction was attempted on the specimens for comparison to x-ray diffractions of untested specimens. Corrosive resistance was tested by the 24-hour immersion in a continuously agitated 16% HF solution of specimens for which careful measurements of weight, density, and porosity had been made. In addition to after-test measurements, to

determine changes in these three items, the specimens were sliced longitudinally for microscopic observation and the outer layer produced by corrosion was powdered for x-ray diffraction.

3. Thermal Expansion. Coefficients of thermal expansion were determined by the dilatometric method.

F. X-Ray Diffraction. A Philips Norelco diffractometer with Cu K-alpha radiation, operated at 40 kv and 20 Ma, was used for making powder diffraction patterns of specimens both in the as-received condition and after test. Specimens were crushed, then ground to less than 320 mesh size in a Dia-mon-ite (primarily alumina) mortar. Where there was an insufficient volume of material for powdering (e.g., surface layers formed during high temperature exposure), diffraction of the solid was undertaken.

C. Microstructural Observation. Optical viewing of specimens before and after testing was done on a Zeiss Metallograph. An AMR Scanning Electron Microscope was also used. Polishing of specimens for microstructural observations was done through successive series of SiC papers, diamond impregnated polishing wheels, and vibrators down to 1/4 micron grit size. An etchant mixture of 10 ml HF (45% sol), 10 ml HNO_3, and 10ml Glycerol was used. Etching times were successively reduced from an initial time of three minutes to a final time of approximately 5 seconds as experience was gained.

H. Electron microprobe Analysis. An electron microprobe analysis for Al:Si ratios was conducted as further verification of the composition of the materials being investigated. Two Bakelite mounts, each containing one specimen of the four materials, were prepared. Surfaces were polished to 0.25 um diamond grit. Al_2O_3 and SiO_2 standards were used

and standard Al and Si counts were established before and after scanning each set of specimens. Al:Si ratios were calculated from the raw data from the solid solution matrix. The raw data were also computer processed using a program designed to provide average Si and Al contents in atomic percentages for each specimen probed, after correcting for absorption, fluorescence, atomic number, dead time drift and background. A Model 400 electron microprobe analyzer, Materials Analysis Company, Palo Alto, California, was used.

IV. RESULTS AND DISCUSSION

A. Characterization in As-Received Condition.

1. X-ray diffraction. Figure 11 is a composite of the tracings from x-ray powder diffraction patterns of the four materials as-received. The 2θ angles and related d-spacings were compared to those reported in the literature for sialons. With exception of the two minor peaks at 2θ = 47.3° and 74.0°, the M3 and M4 peaks correspond exactly to those reported by Oyama for a Si_3N_4 solid solution (with AlN and Al_2O_3) that was later to be called a β^1-Si_3N_4 sialon[66]. The majority of the M2 peaks, including those of highest intensity, convert closely to d-values given by Jack for the 15R-AlN polytype phase[67]. In addition, there are a significant number of α-Al_2O_3 peaks corresponding to data from ASTM Powder Index Card 11-661. It is obvious from Figure 11 that the M3 and M4 materials have the same crystalline structure and that this structure is not the same as that of the M2 material. Also evident is the fact that the M1 material is a mixture of the M2 and M3/M4 materials, for there are significant β^1-Si_3N_4 peaks matching those in the M3/M4 tracings and 15R-AlN polytype peaks plus Al_2O_3 peaks matching those in the M2 tracing.

2. Chemical Composition. The semi-quantitative spectrographic analysis shown in Table 4 reports the atomic chemical constituents present in the materials as calculated from the reported values for the oxides of the elements indicated. Silicon is present in significant amounts in materials M1 and M2 (18.7 w/o and 11.7 w/o, respectively); it is shown as the principal constituent of materials M3 and M4. Likewise, aluminum is present in significant amounts in materials M3 and M4 (18.5 w/o and 13.2 w/o, respectively) while it is shown as the principal

constituent of materials M1 and M2. In considering chemical composition, therefore, the materials may be grouped according to principal constituents: M1/M2 (principal constituent Al) and M3/M4 (principal constituent Si).

Two general chemical formulae may be applicable to this grouping. The first, $Si_{6-x}Al_xO_xN_{8-x}$, has been shown by the literature survey to be generally accepted as representing the composition of the β-Si_3N_4-Al_2O_3-AlN sialons. The second formula arises from Jack's representation of the sialon system in the manner of Gauckler, et al (see Fig. 8) as a quaternary system (Si_3N_4-AlN-Al_2O_3-SiO_2). He has identified the X_2 phase of Gauckler, et al, as the 15R-AlN polytype sialon[64]. Based on Jack's representation, the composition of the 15R-AlN polytype phase could be approximated by

$$Si_{(1.1 \text{ to } 0.4)}Al_{(3.5 \text{ to } 2.5)}O_{(1.2 \text{ to } 2.0)}N_{(3.2 \text{ to } 2.7)}$$

with the composition of the center of the 15R region as shown by Jack being $Si_{0.75}Al_3O_{1.5}N_3$. It is noted that the Al:Si ratios for the 15R phase, by this representation, range from about 3:1 to 6:1.

Assuming the materials in question to be solid solutions of compositions falling within one or the other of these two general formulae, there remains the question of what other phases might be present, as intermediate or metastable phases, as the result of chemical reactions during firing involving not only the SiO_2 and Al_2O_3 initially present in the volcanic ash, but FeO-Fe_2O_3, CaO, MgO, K_2O, and Na_2O as well. It is suggested that the oxides -- of Ca, K, and Na in particular -- have reacted with SiO_2 to form a glassy phase or phases. This is in accordance with reports in the literature that glassy phases are normally found in sialons. The additional compounds need not all by amorphous.

As mentioned in the literature survey, Gauckler, et al, reported mullite and several crystalline x-phases as well as sialons present in the Si_3N_4-AlN-Al_2O_3-SiO_2 system at or slightly above 1700 °C which was the reported firing temperature of materials M2, M3, and M4.

3. Electron Microprobe Analysis. The results of an electron microprobe analysis for Al:Si ratios in each material are shown in Table 5. Ratios selectively calculated from raw data are for the matrix in each case, while ratios obtained by computer processing of the raw data are overall averages taking into account the relative Al:Si content of the visible, discrete particles scanned by the microprobe. (At the 400X magnifying power of the probe microscope a grain structure was not visible, but numerous distinctive particles were crossed in scanning.) The results conform with those reported for chemical composition and x-ray diffraction. M2, the most dense material, is shown by the microprobe to have the highest Al:Si ratio (5 or 6:1). This is consistent with the approximate formula given for the 15R-AlN polytype phase in which the range of Al:Si ratios is 3:1 to 6:1. Also, it corresponds to x-ray diffraction results for M2, which show a predominance of crystalline aluminum compounds present, and to the spectrographic analysis which shows M2 having Al as the principal constituent, somewhat less Si than M1, and much less Si than M3 and M4. The next most dense material, M1, shown by the microprobe to have more silicon content than M2 (Al:Si ratio of 1.5:1 to 2:1 versus 5 or 6:1), is revealed by x-ray diffraction to have some peaks representing Si compounds as well as numerous peaks representing Al compounds. This is consistent with the spectrographic analysis. M3 and M4 are shown by the microprobe analysis to have nearly equivalent Al:Si ratios with that for M3 being slightly more than the

ratio for M4. This corresponds to the x-ray diffraction results, which show equivalent crystalline structures, and to the spectrographic analysis which shows a somewhat higher Al content, hence a somewhat higher Al:Si ratio, for the M3 material.

Further consideration of the data in Table 5 shows that the difference between computer results and calculations from raw data, which ignore specific particle counts, is greatest for the M1 material. It is considered that this reflects the more complex structure of the M1 material; i.e., there are more phases, some of which may have shown up as distinctive particles whose counts (although Si and Al counts) were not considered in calculating the Al:Si ratio from raw data. For the M2, M3, and M4 materials, the computer results are closer to the raw data calculations. This indicates that these materials are more homogeneous solid solutions than the M1 material.

4. Density and Porosity. Table 6 shows the average bulk densities, apparent densities, and open porosities of materials M1, M2, M3, and M4 as measured. M3 and M4 (at 3.07 and 3.08 gm/cm^3, respectively) are well within the 3 - 3.2 gm/cm^3 density range shown in Table 2 for the β^1-Si_3N_4 sialons. M1 and M2 (at 3.2 and 3.35 gm/cm^3, respectively) are at the upper limit or above the β^1-Si_3N_4 density range. These values are consistent with the presence of AlN (at 3.26 gm/cm^3) and Al_2O_3 (at 3.96 gm/cm^3). The compounds of higher silicon content (M3 and M4) would be expected to have lower densities because of their more open structure as compared to the compounds with less silicon and more aluminum content (M1 and M2). All the materials are relatively low in open porosity as shown by the values ranging from 0.19% for M1 to 0.007% for M4. M1 and M2 have greater open porosity than do M3 and

M4. (No significant difference was noted between measurements made on as-cut specimens and as-cut-polished specimens of the same material. This indicates that the pores are closed due to the presence of a glassy phase.)

5. Microstructure. Microstructures of the four materials as-received are shown in Figures 12 through 16. The optical photomicrographs in Figure 12 were selected for comparison of polished but unetched surfaces; those in Figure 13 were selected for comparison of the effects of etching each material for a given length of time. In both cases, the specimens of each material were mounted in a single mount and thus given the same preparatory treatment. The scanning electron photomicrographs in Figure 14 are included to give an indication of the basically rod-like nature of the solid solution sialon microstructure. The scanning electron micrographs, and accompanying energy dispersive analysis by x-ray (EDAX) plots in Figure 15 show evidence that some of the impurities in the starting mixture (i.e., in the volcanic ash) are still present in the M1 material. Figure 16 is a scanning electron micrograph that shows the morphology of particles in the microstructure of the M1 material.

As may be seen in Figure 12, the polished, unetched surfaces of the M1 and M2 materials (A and B, respectively) are quite similar to each other as are the polished, unetched surfaces of M3 and M4 (C and D, respectively). This is consistent with the M1/M2 and M3/M4 grouping suggested by the spectrographic analysis, x-ray diffraction, and electron microprobe scanning. Further, the M1 and M2 materials appear to be multiphase while the M3 and M4 materials appear essentially single phase; this is in further agreement with previous results. Also, the

open porosities as indicated in the photomicrographs agree, relatively, with those reported in Table 4.

Hydrofluoric acid, which attacks silica vigorously but has little effect on aluminum compounds, was a major constituent of the etchant used. From the observation of Figure 13, it appears likely that the HF has attacked the microstructure of the materials in differing degrees depending upon their relative silicon content. The surfaces of M3 and M4 (C and D, respectively) appear to be etched equally, as between the two materials, and uniformly throughout. The surfaces of M1 and M2 (A and B, respectively) both appear to be more affected by the etchant than are the surfaces of the M3/M4 materials. Also, M1 seems to be more deeply etched than is M2. According to Table 13 (as discussed later) M3 and M4 materials are in fact etched more than the aluminum-rich M1 and M2 materials but this attack is not evident in the optical photomicrographs. This is because the M3 and M4 materials, which have been identified as basically single-phase materials (whose principal constituent per Table 4 is silicon), would be expected to etch equally and uniformly throughout the surface area, thus producing little surface contrast. The M1 and M2 materials (A and B, respectively) have been identified as multiphase materials with aluminum as the principal constituent but with some silicon content. It is reasonable to assume that the different phases in these materials would etch differently and thus produce light contrast such as that evident in Figure 13. The fact that M1 appears more heavily etched than M2 is consistent with Table 13 and reflects the higher silicon content reported for M1 in Table 4.

The scanning electron micrographs in Figure 14 reveal, in the

microstructure of each of the materials, the characteristic rod-like morphology of the sialons. There appear to be, at the same time, differences as between the M1/M2 materials (A and B, respectively) and the M3/M4 materials (C and D, respectively). At the same magnification, the individual rods appear larger in the M1/M2 materials than in the M3/M4 materials. Also, there are apparent differences between the M1 and M2 microstructures which could reflect the presence of the β^1-Si_3N_4 phase which the x-ray diffraction indicated to be present in M1 but not in M2.

Figure 15 shows the continued presence in the M1 sialon of impurities that were in the volcanic ash in the starting mix for the M1 material. This conforms with the analysis in Table 4. The EDAX plot in C in the figure was taken of the large pore shown in the upper center of the micrograph at A; the plot in D was taken of the highlighted pore shown in B. The major peaks, in order from left to right, in C are of Al, Si, Ca, and $Fe_{(K\alpha \text{ and } K\beta)}$. The plot at D tends to confirm reports in the literature such as that of Wills, et at, that elemental Si may be found in sialons associated with Fe impurities[68].

The result of heavy etching of an M1 specimen are shown in the scanning electron micrograph in Figure 16. Of the phases indicated by x-ray diffraction to be present in the M1 material, it is considered that most of the β^1-Si_3N_4 and glass phases have been etched away in this case. The generally round and dark areas remaining of the polished surface have, on close inspection, the characteristic rod-like appearance shown in Figure 14. There are also, however, many other rod-like particles not associated with the remnants of the polished surface that could also be sialon rods. There are a few bottle-shaped particles,

larger than the sialon rods, which could be alumina.

These microstructural observations (on Figures 12-16, incl.) may be considered in sum as confirming other experimental results on the characteristics of the materials being investigated.

6. Thermal Expansion. Linear thermal expansions of the four materials up to about 700 °C are shown in Figure 17. These curves conform closely to those of Wills, et al, up to this temperature, for three different sialons investigated by them[69]. Calculated average values for the expansion coefficients are shown in Table 7 and range from 2.77 x 10^{-6}/°C to 3.25 x 10^{-6}/°C. These values are slightly lower for three of the materials than those calculated by Wills, et al, but are generally within the range of those reported in the literature as shown in Table 2.

Having investigated thermal diffusivities as well as linear expansions, Wills, et al concluded that the thermal properties of the sialons were invariant with composition[70]. Hendry, et al, in discussing β^1-magnesium sialon, found that its expansion was identical with that of β^1-sialon without magnesia added. They reported that the thermal expansion of sialons was linear within experimental error[71]. The results in this case show little difference in thermal expansion as between the M2 and the M3/M4 materials. The rather small variation shown for the M1 material could be due to experimental error; a specimen of smaller cross-section was used in the dilatometer than was used for materials M2, M3, and M4. Thus, the results from this investigation could be considered as being consistent with the conclusion of Wills, et al, and the report of Hendry, et al that thermal expansion does not change with composition. With respect to the expansion being linear,

as concluded by Hendry, et al, the results as plotted in Figure 17 (and the results of Wills, et al) do not indicate this to be the case. This could be due to experimental error, although the Metals and Ceramics Information Handbook shows a curvilinear relationship[72].

B. Characterization from Mechanical Tests

1. Machineability. A detailed report on relative machining difficulty of the materials is set forth in Table 8. The M3 material was the hardest to cut. M4, M2, and M1 materials were next hardest in that order. The high silicon content in the M3 and M4 materials must be responsible for the machining difficulty. Presumably, there are hard silicon compounds formed on the surface during the hot-pressing operation. That these are surface compounds is deduced from the fact that cutting became easier for the M3 and M4 materials after penetration of the surface layer; this difference was not noticed in the case of the M1 and M2 materials. These results are consistent with the point made by Rice and Speronello that machining difficulty increases as hardness increases[73]. There is much discussion in the literature on the difficulty of machining and the danger of introducing stress-raising flaws. Mechanical test results considered abnormal have been attributed frequently to flaws introduced during the machining of specimens. In this connection, it is appropriate to recall the suggestion by Hasselman and Chen that efforts directed toward improving long thermal fatigue life in silicon nitride (and sialon) should concentrate on controlling mechanisms responsible for crack growth rather than on decreasing initial flaw size[74].

2. Microhardness. The results of microhardness tests are shown in Table 9. Initially, it was planned to have a much more extensive

testing of hardness values, for example those measured after the various mechanical tests. This more extensive testing was precluded, however, by the great difficulty in preparing specimens in order to get consistent hardness readings. Only specimens from the M2 material showed consistent values regardless of method of specimen preparation. It is also difficult to compare these results with results obtained by others because of the variables involved such as different types of testing machines used and different loads at which readings were taken by different investigators. The testing in this case was done on a Vickers microhardness tester, for example, while the one hardness value shown for sialon in Table 2 resulted from testing on a Knoop hardness tester. This experience confirmed in part the points of Coe, et al, that consistent results require special preparation techniques[75]. From a characterization standpoint the results in Table 9 tend to confirm the existence of hard surface layers on materials M3 and M4.

3. Compressive Strength at High Temperature. Figures 18 through 21 are stress-strain curves showing performance of the materials under compression at high temperatures. It is seen that the M2 material is the strongest at all temperatures, exhibiting a strength of at least 116 ksi at 1300 °C (Figure 19). The fact that all specimens fractured at 1200 °C (Figure 18) indicates that at or below this temperature there is little or no accommodation by the materials to the compressive stresses, and thus they act in a brittle fashion. At 1300 °C (Figure 19), the M2 material exceeded the capacity of the test machine and its curve showed a larger slope indicating greater refractoriness. The stress-strain relationship for the M1, M3, and M4 specimens was similar until about 65 ksi at which point the M1 material lost strength rapidly. At

the 1400 °C testing temperature (Figure 20), the M1 material was able to withstand a stress of only about 24 ksi. M3 and M4 specimens showing an almost identical strain for given stresses, achieved a stress value of about 50 ksi at this temperature. The M2 material again was the strongest, reaching a stress of almost 100 ksi at 1400 °C. Because of this performance, an M2 specimen was also tested at 1500 °C. At this temperature, however, the material lost its ability to resist compression, with a gradual and extended plastic flow setting in at about 20 ksi stress. A plot of the stress at 0.2% strain versus temperature for the compressive testing accomplished gives some information on the relative elastic strength of these types of materials. The result is shown in Figure 22. This plot shows that the yield stress of the M1, M3, and M4 materials falls off rapidly with increasing temperature in the range of 1200 °C to 1400 °C. However, the yield stress for the M2 material does not begin to fall off rapidly until 1400 °C.

No data were found in the literature on high-temperature compressive testing of sialon. It was not possible, therefore, to make comparisons of the results here reported to results of other investigators.

An attempt was made to obtain x-ray diffraction patterns of the surface layers formed on the specimens during compressive testing. Difficulty was experienced because of the small size of the specimens and the relatively small amount of surface layer formed; i.e., there was insufficient material to powder, and diffraction data were thus obtained off the surfaces of the small solid specimens. In general the results showed that the crystalline structure of the materials was not changed from that in the as-received condition. There was a general reduction in strength of peaks representing the various

crystalline phases and some peaks previously in evidence did not appear. This may be attributed to the small size of the specimens and preferred alignments; in those cases where considerable plastic strain took place, to the masking effect of the presence of glass on the surface. Overall compressive test data are in Table 10.

4. Bending Strength at Room Temperature. Bend tests at room temperature showed M2 as the strongest material, followed by M1, M4, and M3 in that order (Table 11). Although the M3 material showed greater strength when a rectangular (versus square) cross-section was used for the specimen, systematic effects of geometry on specimen strength were not evident. As noted in the Experimental Procedures section, alumina specimens of different geometry were also tested in order to generate data on the geometrical influence in materials other than sialon. The results for Al_2O_3 were also not considered conclusive; i.e., 42.2 ksi for a square cross-section versus 43.4 ksi for a rectangular cross-section. The 20-43.6 ksi range of values for all specimens tested, with either square or reactangular cross-sections, falls within that shown in Table 2 for sintered sialons (20-45 ksi) but falls well below the reported maximum of 120 ksi for hot-pressed sialons. The M1/M2 materials appear to be stronger than the M3/M4 materials in room temperature bending, in the as-received condition.

5. Bending Strength at Room Temperature after Thermal Shock. Also shown in Table 11 are the results of bending tests made at room temperature following the thermal shocking of specimens by dropping them from a 400 °C anneal into water at room temperature. This treatment severely reduced bending strength at room temperature except in the case of the M4 material which showed a strength of 20 ksi after

thermal shock versus 25 ksi before thermal shock. The M2 material, which was the strongest in bending in the as-received condition (43.6 ksi), exhibited a strength after thermal shock of 18.4 ksi, just under that of the M4 material. The average strength after thermal shock for the M1, M2, and M3 specimens, considering possible experimental errors, were essentially the same. It is interesting to note that the strength of the M1 specimen thermally shocked from 1000 °C (19.2 ksi) is over twice that after being thermally shocked from 400 °C. There is also a considerable difference in the results for the M2 specimens tested after thermal shock, 18.4 versus 8.0 ksi. The scattering of values and the fact that only a limited number of samples were tested make it difficult to draw conclusions as to the relative strength after thermal shock of the aluminum rich materials, M1 and M2, versus the silicon-rich materials, M3 and M4. If another M4 specimen had been tested after thermal shock, it might have exhibited a low enough strength to bring the average for that material down to the 12.6 ksi average of the similar M3 material. This would have resulted in the silicon rich materials being somewhat weaker after thermal shock than the aluminum rich materials. One fact that is evident, however, is that the aluminum rich materials are affected much more severely by thermal shock than are the silicon rich materials -- 61% and 70% reductions for M1 and M2, respectively, versus 37% and 20%, respectively, for the M3 and M4 materials. No data were found in the literature on thermal shock of this type. Hence, it is not possible to compare these results with those of others.

6. Effects on Microstructure of Mechanical Testing. At a testing temperature of 1200 °C, the compressive specimen of the M1 material

fractured at a stress of 79 ksi and at a strain of about 4%. The scanning electron micrograph of one of the fracture surfaces, Figure 23, shows a possible glassy intergranular phase. The white area visible along part of the ridge which runs diagonally across the picture could be amorphous silica. Many small pores are in evidence indicating that the crack front probably spread extremely rapidly through this area. Figure 24 is a scanning electron micrograph of a polished section of one of the broken pieces. It indicates that the basic structure has not changed at 1200 °C and at the fracture stress, at least in this portion of the specimen. The elongated, sialon type grains remain. The grain structure appears to be less dense, however, which suggests that a glassy phase could have been present but diffused or flowed, under high temperature compression, to help form the after-test coating on the outside of the specimen.

At 1300 °C the M1 material exhibited an intermediate strength in compression of 66 ksi at a strain of about 3%. The specimen was unloaded when relatively rapid plastic flow set in at the maximum stress point. There were no observable differences in the microstructure of this specimen after test from the microstructure of the 1200 °C specimen after test. Compression of the M1 material at 1400 °C resulted in a maximum stress of only 23.8 ksi. At this temperature the material exhibited extensive plasticity. The test was stopped at a total of 8% strain at which point the stress was 12.5 ksi. Figure 25A is a photograph showing how the specimen barreled, as the result of the plastic flow under stress, and acquired a mottled glassy surface appearance. The scanning electron micrograph in Figure 25B is a sectional view of the specimen showing the extent of the surface layer. The optical

photomicrograph, Figure 25C, taken with cross-polarized light, shows the surface apparently consisting of many crystalline particles held together by a glassy phase. The scanning electron micrograph in Figure 25D indicates that the internal structure of the M1 specimen, in this case, has changed from one dominated by the elongated, sharply defined particles (typical of the material in the as-received condition) to an unstructured mass of very small particles in a glass-like matrix. Thus, although the sialon rod structures still present must be hidden in the glassy matrix, it appears that at 1400 °C the glassy phase or phases in the M1 material liquify and permit extended plastic flow through grain boundary sliding.

The M2 material exhibited the greatest strength in compression at all temperatures, fracturing only during the test at 1200 °C. It might have fractured at 1300 °C, but it was necessary to stop the test at a stress of 116 ksi due to equipment loading limitations. The specimens tested were not noticeably barrelled and the surface layer was very much less in evidence than on the tested M1 specimens. In Figures 26A, 26B, and 26C, are scanning electron micrographs showing the internal microstructure after testing at 1200 °C, 1300 °C, and 1400 °C, respectively. The microstructure appears to be more glassy at the successively higher temperatures. In Figure 26A (after 1200 °C test) the sialon rods are still quite visible They are less evident in Figure 26B (after 1300 °C test). After the 1400 °C test (Figure 26C) there is little evidence of the sialon rods, but there is still a coherent appearance to the microstructure which is in accordance with the fact that the material is still strong in compression at this temperature. An interesting aspect of the micrographs in Figure 26 is the overall fibrous

appearance of the microstructures. This has been referred to by Jack and Kobayashi as characteristic of the 15R-AlN polytype phase which is the principal phase in the M2 material[76,77]. Also, had the size of the billets received permitted, it would have been interesting to cut and test compressive specimens with their long axis parallel to the pressing direction, rather than perpendicular as was done for the present tests. This would have provided a check on whether fiber alignment made the significant strength difference in compression that Lange reports it made during flexural strength tests; i.e., specimens cut and stressed perpendicular to the hot-pressing direction were stronger[78].

The M3 and M4 materials exhibited almost identical compressive behavior at the three testing temperatures. This similarity in strength is perhaps indicated by the similarity in microstructures as shown in the scanning electron micrographs (Figure 27) of specimens of M3 and M4 after testing at temperatures of 1300 °C and 1400 °C. 1200 °C microstructures are not available as in each case the specimen fractured almost explosively, leaving only very fine particles. In each of the micrographs in Figure 27, there is evidence of the sialon rod-like structure. There is also evidence of rather large open pores which were probably closed prior to testing by the glassy phase (it will be recalled that the M3 and M4 materials had the lowest percentage open porosity in the as-received condition).

The observations of the effects on microstructure of compressive testing tend to confirm theories discussed in the literature survey. These propose that plastic deformation of the sialons takes place through grain boundary sliding facilitated by the presence of

intergranular glassy phases which flow under pressure at high temperatures.

Study of the microstructures of specimens after room temperature bend testing, including those of specimens thermally shocked before testing, revealed in all cases a brittle fracture mode with fairly obvious flaws at fracture initiation points. Except in the case of the M4 specimen tested after thermal shock, there were no discernible differences in the overall textures of the fracture surfaces; the fracture surface of the M4 specimen in question was exceptionally smooth over three-quarters of its area. Also, there were no discernible differences between the M1/M2 and M3/M4 fracture surfaces. No photomicrographs of the M1 and M2 specimens are available, but the scanning electron micrographs in Figures 28-31, inclusive, are illustrative of all the bending fracture surfaces.

Figure 28 includes scanning electron micrographs of an M3 specimen which failed in room temperature, 4-point bending at 20 ksi. The fracture surface shows a typically brittle fracture mode with weakening inclusions evident at one corner where the fracture line starts. Of particular interest is the white outline where the arched fracture line jogs around a possible residual silicon particle in the structure. In studying fracture resistance of silicon nitride, Barnby and Taylor discuss residual silicon particles and their effect[79]. They noted that the residual silicon appeared as a white phase and reported that fracture paths circumnavigated silicon particles. In a sialon with excess silicon, it is reasonable to assume that a similar event might occur. The spherically shaped particle at the upper right in the lower photograph in Figure 28 is similar to others observed (in an M1

compressive fracture surface) that were identified by EDAX as iron.

Figure 29 is a scanning electron micrograph of an M4 specimen fractured at room temperature in 4-point bending (the tensile surface is at the top in the photograph). This reveals, on the corner shown, a flaw from which the fracture probably originated. The remainder of the photograph is typical of the overall fracture surface, showing brittle fracture.

Figure 30 is an end view of the fracture surface in bending of an M3 specimen that had been thermally shocked prior to testing. The tensile surface is at the top of the photograph as viewed. Of interest in this microstructure is the triangular shaped white area in the center. It appears that fracture may in this case have originated from this internal area rather than from a surface flaw. Also of interest are the white lines to the left of the white area as viewed. It is suggested that both the white area and the white lines are residual silicon.

The fracture surface of an M4 specimen thermally shocked and then tested in bending at room temperature is shown in Figure 31. In view of the fact that this surface is so smooth in most areas, and apparently intergranular, it is surprising that the specimen exhibited the highest strength of those tested after thermal shock. There is, however, evidence of slow crack growth as indicated by the terrace-like steps in the areas marked 1, 2, and 3 on the micrograph. At the test loading rate, this slower crack growth may have produced the higher strength result for this specimen. It appears that once the leading edge of the fracture passed the area marked 3 (tensile surface at upper left), the crack progressed very rapidly and in a brittle fashion through the

remainder of the cross section.

In connection with the bend tests, it is interesting to speculate on what strength would have been exhibited by the M1 square-cross-section specimen if it had been tested at the same loading rate as the others. Davidge, et al state that there is an inverse strain rate dependence on strength, and that specimens tested at low strain rates are stronger than those tested at high strain rates, where the time available for crack rounding is less[80].

C. Characterization from Other Tests

1. Oxidation Resistance. As described in the Experimental Procedures section, tests for oxidation resistance were carried out by placing specimens in the furnace used for high temperature compressive testing while tests at 1400 °C were underway. The oxidation specimens were in this manner exposed to a temperature of 1400 °C for periods of approximately three hours. Low magnification observations of the specimens after oxidation were as follows: (1) M1 - dimensions appeared unchanged, exposed surfaces appeared to be covered with a glassy layer of white to red-brown color, open pores appeared through the surface layer in some places; (2) M2 - dimensions appeared unchanged, exposed surfaces appeared to have a very thin surface layer resulting from oxidation; (3) M3 - practically no oxidation was evident; (4) M4 - no oxidation evident. These observations were then considered in the light of weight measurements and scanning electron microscope observations. Table 12 shows the weight gains for the four specimens. All weight gains are low although that for specimen M2 (8.3 mg/cm^2) is considerably higher than the gains for the M1, M3, and M4 specimens. Figure 32 shows scanning electron micrographs of the surfaces. These

micrographs in each case are representative of the surfaces directly exposed.

For the M1 and M2 specimens little open porosity is evident, indicating that the oxidation layer probably did not experience cracking or shrinking during cooling. There appear to be some free surface particles present on both of the M1 and M2 surfaces.

By contrast to the M1 and M2 surfaces, open pores are very much in evidence in the micrographs of the oxidized surfaces of the M3 and M4 specimens. Also, scattered, possibly spherical particles are a part of the M3 and M4 surfaces. They appear to be covered by the continuous glassy film that surrounds the visible pores.

Separate or possibly free surface particles appear in the M1, M2, and M3 specimen micrographs, but are noticeably absent from the M4 surface. Attempts to identify these particles by EDAX were unsuccessful. Some may have been introduced in handling, but the remarkably clean surface of the M4 specimen, which received the same handling as did the other specimens, argues that they either were in the microstructure before oxidation or became isolated at the surface during oxidation. Specimen M3, and to a very slight extent M4, reveal particles in the center of some pores. It is suggested that these could be sialon particles that were present in the microstructure prior to oxidation.

X-ray diffraction revealed a crystalline content for all surfaces following oxidation. Included in the oxidation products identified by diffraction were mullite on the M1 surface, mullite plus a trace of cristobalite on the M2 specimen surface, and about equal amounts of mullite and cristobalite on the M3 and M4 surfaces.

The very low weight gain shown in Table 12 for the M3 and M4

materials is consistent with reports in the literature on oxidation of β^1-Si_3N_4 sialons. Schlichting et al refer to the formation of a mullite and cristobalite surface layer during oxidation of a β-$Si_{6-x}Al_xO_xN_{8-x}$ sialon and conclude that this layer inhibits further oxidation[81]. They also report that increased Al content (within the $Si_{6-x}Al_xO_xN_{8-x}$ composition range) results in increased oxidation resistance. The much higher weight gain for the M2 material, although it contains more aluminum than the β^1-sialons, suggests that its different Si-Al-O-N composition rnage and different structure lower its oxidation resistance. The intermediate weight gain for the M1 material as shown in Table 12 would thus be explained. The β^1-sialon phase that it contains would make it more oxidation-resistant than the M2 material, while its AlN polytype phase would make it less resistant than the M3/M4 materials.

2. Corrosion Resistance. As shown in Figure 33, all specimens exhibited a weight loss when subjected to immersion in a 16% HF solution for even a short period of time. Only specimen M2 was recognizable at the end of four hours treatment, by which time M3 had lost more than 23% weight while M4 had lost 21%. At the end of 24 hours M1 had lost 40% weight while M3 and M4 had lost nearly 80% of their original weight (see Table 13 for details). Turkdogan, Bills, and Tippett noted the weight loss when silicon nitride was reacted with HF[82]. Hydrolysis of silicon nitride in aqueous hydrofluoric acid eventually goes to completion, according to Colquhuon, et al, if the acid concentration is maintained above 19 w/o[83]. The acid solution in the present test was 16 w/o HF, and it had a corrosive effect on the M1, M3, and M4 materials which contained β^1-sialon. M2, which contained the

AlN type was the least affected. This corrosion test result was presaged by the earlier experience of the effects on the materials of etchant containing HF. It remains to be seen how the sialons will resist corrosion in environments not containing HF acid. The literature is silent on the subject except for general statements that sialons are resistant to corrosive environments.

V. SUMMARY AND CONCLUSIONS

Four sialon-type materials using volcanic ash as a raw material were characterized and some of their properties were determined. The M3 and M4 materials were identified as β^1-Si_3N_4 sialons; their principal constituent is silicon. The M2 material was identified as a 15R-AlN polytype sialon whose principal constituent is aluminum. The M1 material is a mixture of the two types. Table 14 is an overview of results showing the general structural formulae and the relative order of the materials with respect to various properties as determined by the investigation.

The materials generally may be characterized as follows: they have high melting points and low open porosities; they are very hard, and have low range of coefficients of thermal expansion, high compressive strengths at elevated temperatures, and fair room temperature bending strengths. Characteristically, their deficiences from an engineering applications standpoint are fabrication/machining difficulty, relatively low thermal shock resistance, susceptibility to HF corrosion, and brittle fracture modes. The M2 material appears to be the most favorable and warrants continued investigation.

The microstructural studies of the materials as received indicate a basic rod-like grain as characteristic of sialons with a glassy phase or phases distributed rather uniformly throughout the structure. This rod-like particle is the basic β-Si_3N_4 structure extended in the c-direction with solid solution of AlN and Al_2O_3. The composition of the glassy phase or phases reflects the impurities in the starting mix.

Mechanical test results, together with microstructural observations, indicate that the basic β^1-Si_3N_4 and 15R-AlN polytype phases retain

their identity during compressive testing at high temperatures. The nature of the response of the glassy phase to temperature and pressure determines whether the material will fracture in brittle fashion or deform plastically. The stress-strain data indicate that below the softening point of the glassy phase, the material fractures in a brittle fashion of intergranular failure under a stress exceeding the strength of the bond between the glass and the sialon grains. At a temperature sufficiently high to soften the glass, grain boundary sliding takes place facilitated by viscous glassy layers beteen grains, and the material deforms plastically under stress. Within this context, and on the basis of the stress-strain data, it is postulated that the 15R-AlN polytype phase (M2 material) is stronger in compression and bending (other than after thermal shock) because of a more refractory and smaller amount of glass phase due to its greater aluminum content. There was insufficient test data to provide an explanation as to why the M1 and M2 materials are percentage-wise affected much more than the M3 and M4 materials by thermal shock.

It is concluded that of the materials tested, the M2 material shows the most promise as a candidate for meeting some of the current needs for high-temperature materials. It is also concluded that more research is needed in order to explain the low resistance of these materials to thermal shock since their coefficients of thermal expansion are relatively low.

ACKNOWLEDGEMENTS

I am most grateful to Professor Joseph A. Pask for offering me the opportunity to do this work under his supervision. He has been most patient and extremely helpful.

Professor Richard M. Fulrath provided valuable assistance in the x-ray and dilatometric work. Thanks are also due Professors Earl R. Parker and Victor F. Zackay for their encouragement, and to Professor Alan W. Searcy for joining my thesis committee on short notice in the emergency absence of another member. Special thanks are due Professor Robert H. Bragg for his early inspirational guidance.

My colleagues, Glenn A. Holmquist and Philip C. Dokko offered valuable advice and encouragement. Michel D. Sacks gave particularly helpful advice on the high temperature compressive testing work.

The technical assistance of the support staff of the Materials and Molecular Research Division, Lawrence Berkeley Laboratory was greatly appreciated. I wish to thank Lee Johnson (optical microscopy assistance), Rich Lindberg (SEM and electron microprobe assistance), Ed Edwards (machine shop assistance) and Gloria Pelatowski (technical drawings). My sincere thanks to Jenni Ingraham for her most efficient and rapid preparation of the manuscript.

Grateful acknowledgement is made to the U.S. Energy Research and Development Administration, Division of Physical Research, through the Materials and Molecular Research Division, Lawrence Berkeley Laboratory, for use of facilities and equipment.

REFERENCES

1. Cochran, N. P., "Oil and Gas from Coal," Scientific American, 234 (5), 24-29 (1976).
2. Hauck, W. E., "Future for Ceramic Gas Turbine Design", Gas Turbine World, Sept. 1974.
3. Ibid.
4. Jack, K. H. and Wilson, W. L., "Ceramics Based on the Si-Al-O-N and Related Systems," Nature (Phys. Sci.) 238 (7), 28-29 (1972).
5. Oyama, Y, and Kamigaito, O., "Solid Solubility of Some Oxides in Si_3N_4", Japan J. Appl. Phys. 10 1637 (1971).
6. Umebayashi, S., and Kobayashi, K., "Materials Reaction-Sintered from Volcanic Ash and Al Powder in N_2", Amer. Ceram. Soc. Bull., 54 (5) 534 (1975).
7. Umebayashi, S. and Kobayashi, K., "β-Si_3N_4 Solid Solution Prepared from Volcanic Ash and Al Powder in N_2", J. Amer. Ceram. Soc., 58 (9-10) 464 (1975).
8. Lee, J. G., Casarini, R., and Cutler, I. B., "Sialon Derived from Clay to Provide an Economical Refractory Material", J. Heat Technology, Industrial Heating, 43, 50-53 (1976).
9. Croft, W. J. and Cutler, I. B., "Review of Silicon Nitride", Dept. of Army, E. R. P. Report No. 2-73 and Dept. of Navy, ONR Report No. R-16-73, 4-5 (1973).
10. Vassilou, B. and Wilde, F. G., "A Hexagonal Form of Silicon Nitride", NATURE (London) 179.1, 435-436 (1957).
11. Popper, P., and Ruddlesen, S. N., "Structure of the Nitrides of Silicon and Germanium", NATURE (London) 179.2 1129 (1957).
12. Hardie, D. and Jack, K. H., "Crystal Structure of Silicon Nitride" NATURE, 180, 332-333 (1957).
13. Turkdogan, E. T., Bills, P. M., and Tippett, V. A., "Silicon Nitrides: Some Physico-Chemical Properties", J. Appl. Chem. 8 296-301 (1958).
14. Thompson, D. S., and Pratt, P. L., "The Structure of Silicon Nitride", Science of Ceramics 3, ed. by G. H. Stewart, Academic Press, New York, 33-51 (1967).

15. Wild, S., Grieveson, P., and Jack, K. H., "The Crystal Structures of Alpha and Beta Silicon and Germanium Nitrides", Special Ceramics 5, 385-395 (1972).

16. Oyama, Y., and Kamigaito, O., "Solid Solubility of Some Oxides in Si_3N_4, Japan J. Appl. Phys. 10, 1637 (1971).

17. Oyama, Y., "Solid Solution in the Ternary System, Si_3N_4-AlN-Al_2O_3" Japan J. Appl. Phys. 11, 750-751 (1972).

18. Jack, K. H., and Wilson, W. I., "Ceramics Based on the Si-Al-O-N and Related Systems", Nature Physical Sci. 238, 28-29 (1972).

19. Umebayashi, S., and Kobayashi, K., Op. Cit. (see reference 6).

20. Umebayashi, S., and Kobayashi, K., Op. Cit. (see reference 7).

21. Gauckler, L. J., Lukas, H. L., and Petzow, G., "Contribution to the Phase Diagram Si_3N_4-AlN-Al_2O_3-SiO_2", Journal of The American Ceramic Society--Discussions and Notes, 58, (7-8), 346-347 (1975).

22. Gauckler, L. J., Lukas, H. L., and Tien, T. Y., "Crystal Chemistry of β-Si_3N_4 Solid Solutions Containing Metal Oxides", Mat. Res. Bull. 11, 503-512 (1976).

23. Lewis, M. H., Powell, B. D., Drew, P. Lumby, R. J., North, B., and Taylor, A. J., "The Formation of Single-Phase Si-Al-O-N Ceramics", J. Mat. Sci. 12, 61-74 (1977).

24. Clarke, D. R. and Thomas G., "Grain Boundary Phases in a Hot-Pressed MgO Silicon Nitride", Presented in part at the Pacific Coast Regional Meeting, the American Ceramic Society, San Francisco, Nov. 3, 1976.

25. Jack, K. H., "Nitrogen Ceramics", Tran. and J. Brit. Ceram. Soc., 72, 276-284 (1973).

26. Croft, W. J., and Cutler, I. B., Op. Cit, (Table III, p. 24).

27. Engineering Property Data on Selected Ceramics, Vol. 1, Nitrides, Metals and Ceramics Information Center, Columbus, Ohio (1976).

28. George, W., "Thermal Property Measurements", Proc. of Brit. Ceram. Soc. 22, 147-167 (1973).

29. Torti, M. L., Alliegro, T. A., Richerson, D. W., Washburn, M. E., and Weaver, G. Q., "Silicon Nitride and Silicon Carbide for High-Temperature Engineering Applications", Proc. of Brit. Ceram. Soc. 22, 129-145 (1973).

30. Godfrey, D. J., and Lindley, M. W., "The Strength of Reaction-

Bonded Silicon Nitride Ceramics", Proc. of Brit. Ceram. Soc., 22, 229-289 (1973).

31. Ashcroft, W., "Mechanical Properties of Silicon Nitride at Elevated Temperatures", Proc. of Brit. Ceram. Soc. 22, 169-179, (1973).

32. Noakes, P. B., and Pratt, P. L., "High-Temperature Mechanical Properties of Reaction-Sintered Silicon Nitride", Special Ceramics 5, Proceedings of the Fifth Symp. on Spec. Ceram. held by The Brit. Ceramic Soc. at Stoke-on-Trent, July 1970, ed. by P. Popper, The Brit. Ceramic Res. Assn., Manchester, England, 299-310 (1972).

33. Coe, R. F., Lumby, R.J., and Pawson, M. F., "Some Properties and Applications of Hot-Pressed Silicon Nitride", Special Ceramics 5, (same meeting as in ref. 32 above), 361-376 (1972).

34. Petrovic, J. J. Jacobson, L. A. Talty, P. K., and Vasudevan, A. K., "Controlled Surface Flaws in Hot-Pressed Si_3N_4", J. of The Amer. Ceram. Soc., 58, (3-4) 113-116 (1975).

35. Ud Din, Salah and Nicholson, P. S., "Creep Deformation of Reaction-Sintered Silicon Nitrides", J. of The Amer. Ceram. Soc., 58, (11-12) 500-502, (1975).

36. Ammann, C. L., Doherty, J. E., and Nessler, C. G., "Failure Prediction of the Thermal Fatigue of Silicon Nitride", J. of The Amer. Ceram. Soc., 58, (11-12) 513-516 (1975).

37. Hasselman, D. P. H., and Chen, E. P., "Role of Activation Energy of Slow Crack Growth in the High Temperature Thermal Fatigue of Silicon Nitride", J. Amer. Ceram. Soc. 60, (1-2) 76 (1977).

38. Barnby, J. T., and Taylor, R. A., "The Fracture Resistance of Reaction-Sintered Silicon Nitride", Special Ceramics 5, (same meeting as in ref. 32 above) (1972).

39. Horton, R. M., "Oxidation Kinetics of Powdered Silicon Nitride", J. of Amer. Ceram. Soc., 52, (3) 121-124 (1969).

40. Kiehle, A. J., Heung, L. K., Gielisse, P. J., and Rockett, T. J., "Oxidation Behavior of Hot-Pressed Si_3N_4", J. of Amer. Ceram. Soc., 58, (1-2) 17-20 (1975).

41. Singhal, S. C. "Effect of Water Vapor on the Oxidation of Hot-Pressed Silicon Nitride and Silicon Carbide", J. of Amer. Ceram. Soc., 59, (1-2), 81-82 (1976).

42. Rowcliffe, D. J., and Huber, P. A., "Hot Gas Stress Corrosion of Silicon Nitride and Silicon Carbide", Special Ceramics 5, (same meeting as in ref. 32 above) 239-259 (1972).

43. Same reference as No. 27.

44. Same reference as No. 18.

45. Yeh, Hun C., Sanders, W. A., and Luttner J. L., "Pressure Sintering of Si_3N_4-Al_2O_3 (Sialon)", Ceramic Bulletin, 56 (2) 189-193 (1977).

46. Wills, R. R., Stewart, R. W., and Wimmer, J. M., "Effect of Composition and X-Phase on the Intrinsic Properties of Reaction-Sintered Sialon", Ceramic Bulletin, 56 (2) 194-196 (1977).

47. Wills, R. R., Stewart, R. W., and Wimmer, J. M. "Fabrication of Reaction-Sintered Sialon", J. of Amer. Ceram. Soc., 60, (1-2) 64-67 (1977).

48. Lumby, R. J., North, B., and Taylor, A. J., "Chemistry and Creep of Sialons", Special Ceramics 6, ed. by P. Popper, Brit. Ceram. Res. Assn., Stoke-on-Trent, England, 283-297 (1975).

49. Same reference as No. 23.

50. Same reference as No. 18.

51. Schlichting, J. and Gauckler, L. J., "Oxidation of Some β-Si_3N_4 Materials", Powder Metallurgy International 9 (1), 36-39, (1977).

52. Lee, J. G., Casarini, R., and Cutler, I. B., "Sialon Derived from Clay to Provide an Economical Refractory Material", Industrial Heating, 50-53, (1976).

53. Lange, F. F., "Dense Si_3N_4: Interrelation between Phase Equilibria, Microstructure, and Mechanical Properties", Final Report, Contract No. N00014-74-C-0284 (1976).

54. Lange, F. F., "Relation Between Strength, Fracture Energy, and Microstructure of Hot-Pressed Si_3N_4", J. of Amer. Ceram. Soc., 56, (10) 518-522 (1973).

55. Iskoe, J. L., and Lange, F. F., "Development of Microstructure, Strength and Fracture Toughness of Hot-Pressed Si_3N_4", Technical Report #7, Westinghouse Elec. Corp. Contract No. N00014-74-C-0284 (1976).

56. Davidge, R. W., Evans, A. G., Gilling, D., and Wilyman, P. R., "Oxidation of Reaction-Sintered Silicon Nitride and Effects on

Strength", Special Ceramics 5, (same meeting as reference 32 above) 329-343 (1972).

57. Evans, A. G., and Davidge, R. W., "The Strength and Oxidation of Reaction-Sintered Silicon Nitride", J. of Mat. Sci 5, 314-325, (1970).

58. Jayatilaka, A. de S., and Leake, J. A., "The Influence of Progressive Oxidation on the Fracture Toughness and Strength of Reaction-Bonded Silicon Nitride at Elevated Temperatures in Air", Pro. Brit. Ceram. Soc. 25, 311-323 (1975).

59. Dalgleish, B. J., and Pratt, P. L., "The Influence of Microstructure on the Reaction-Bonded Silicon Nitride", Proc. Brit. Ceram. Soc. 25, 295-309, (1975).

60. Godfrey, D. J., "The Effects of Impurities, Additions, and Surface Preparation on the Strength of Silicon Nitride", Proc. Brit. Ceram. Soc., 25, 325-337 (1975).

61. Coppola, J. A., Bradt, R. C., Richerson, D. W., and Alliegro, R. A., "Fracture Energy of Silicon Nitrides", Ceramic Bulletin, 51, (11), 847-852 (1972).

62. Seltzer, M. S., "High Temperature Creep of Silicon-Base Compounds", Ceramic Bulletin, 56, (4), 418-423 (1977).

63. Rice, R. W., and Speronello, B. K., "Effect of Microstructure on Rate of Machining of Ceramics", J. Amer. Ceram. Soc., 59 (7,8) 330-333 (1976).

64. Jack, K. H., "Sialons and Related Nitrogen Ceramics", J. Mat. Sci., 11, 1135 (1976).

65. Gauckler, et al, op. cit. (same as Reference 21).

66. Oyama, op. cit., (same as Reference 17).

67. Jack, K. H., op. cit., (same as Reference 64).

68. Wills, et al, op. cit. (same as Reference 46).

69. Ibid.

70. Ibid.

71. Hendry, A., Perora, D. S., Thompson, D. P., and Jack, K. H., "Phase Relationships in the MgO-Si_3N_4-Al_2O_3 System", Special Ceramics 6, ed. by P. Popper, Brit. Ceram. Res. Assoc., Stoke-on-Trent, England, 321-331 (1975).

72. Engineering Property Data on Selected Ceramics, Vol. 1, Nitrides, (same as Reference 27).

73. Rice and Speronello, op. cit., (same as Reference 63).

74. Hasselman and Chen, op. cit., (same as Reference 37).

75. Coe, et al, op. cit., (same as Reference 33).

76. Jack, op. cit., (same as Reference 64).

77. Kobayashi, K., private communication.

78. Lange, op. cit., (same as Reference 53).

79. Barnby and Taylor, op. cit., (same as Reference 38).

80. Davidge, R. W., Tappin, G., and McLaren, J. R., "Strength Parameters Relevent to Engineering Applications for Reaction Bonded Silicon Nitride and REFEL Silicon Carbide", Powder Met., Intl., 8, (3) 110-114 (1976).

81. Schlichting, et al, (same as Reference 51).

82. Turkdogan, et al, op. cit., (same as Reference 13).

83. Colquhuon, I., Thompson, D. E., Wilson, W. I., Grieveson, P., and Jack, K. H., "The Determination of Surface Silica and its Effect on the Hot-Pressing Behavior of Alpha-Silicon Nitride Powders", Proc. of Brit. Ceram. Soc., 22, (6) 181-195 (1973).

Table 1. Some Physical Properties of Silicon Nitride*

Property	Value	Comments
Melting Point	Vaporizes at about 1900°C	
Density	2.2 to 3.2 g/cm^3	depending on method of fabrication
Coef. of Thermal Expansion to 1000°C	2.46 to 4.1 x 10^{-6} °C^{-1}	variation in investigators
Young's Modulus	up to 46 x 10^6 psi 29 x 10^4 MN m^{-2}	depends on fabrication
Mod. of Rupture	up to 125,000 psi 860 MN m^{-2}	depends on fabrication
Thermal Conductivity	up to 20 Btu $hr^{-1}ft^{-1}$°F^{-1} 36 watts m^{-1}°K^{-1}	depends on fabrication
Specific Heat	0.17 cal/g°C 0.712 kJ/kg°C	
Hardness	1600-1800 Vickers VPN >9 (Moh)	
Electrical Resistivity	greater than 10^{10} ohm cm	

*After Croft and Cutler (Ref. 26)

Table 2. Some Physical Properties of Sialon (β'-Si_3N_4)

Property	Value	Reference
Melting Point	Vaporizes at about 1900°C	(27)
Density	3 - 3.2 g/cm^3	(4)
Coefficient of Thermal Expansion	2.7×10^{-6}/°K (x-ray) 3.0×10^{-6}/°K (dilat.)	(4)
Young's Modulus	--	none available through 1976
Modulus of Rupture	Up to 120,000 psi (HP) 20-45,000 psi (sintered) More than 40,000 (sint.)	(27) (27) (4)
Thermal Conductivity	--	none available through 1976
Specific Heat	--	none available through 1976
Hardness	--	none available through 1976
Electrical Resistivity	--	none available through 1976

Table 3. Intrinsic Properties of Sialon Materials*

Property	Value
Hardness (2.6 kg Knoop)	1200 - 1313
Young's Modulus at 20°C (GN/m^2)	231 - 239
Shear Modulus at 20°C (GN/m^2)	90 - 91
Poisson's Ratio	0.26 - 0.29
Critical Stress Intensity Factor at 20°C (MN/m^2)	1.32 - 2.65
Fracture Surface Energy at 20°C ($J/m^{3/2}$)	3.5 - 14.5
Thermal diffusivity (100°C) (cm^2/s)	0.0195 - 0.0313

* Adapted from Wills, Stewart, and Wimmer (Ref. 46)

Table 4: Semi-Quantitative Spectrographic Analysis*

The results shown below are expressed in weight % of elements present. They were calculated from the oxides of the elements detected.

Element		M1	M2	M3	M4
Silicon	(Si)	18.7	11.7	Principal Constituent	
Aluminum	(Al)	Principal Constituent		18.5	13.2
Iron	(Fe)	1.4	1.2	1.0	1.0
Calcium	(Ca)	1.0	0.7	0.4	0.3
Magnesium	(Mg)	0.3	0.2	0.1	0.1
Titanium	(Ti)	0.1	0.03	0.1	0.03
Barium	(Ba)	0.02	0.01	0.01	0.01
Boron	(B)	0.008	0.016	0.008	0.006
Manganese	(Mn)	0.016	0.009	0.006	0.006
Strontium	(Sr)	0.008	0.004	0.004	0.004
Chromium	(Cr)	†0.0006	0.0006	0.002	0.002
Copper	(Cu)	0.006	0.006	0.002	0.006
Nickel	(Ni)	†0.0008	†0.0008	0.005	0.004
Vanadium	(V)	0.002	0.002	0.008	0.008
Tin	(Sn)	0.002	-	-	-
Zirconium	(Zr)	-	-	0.007	0.006
Cobalt	(Co)	-	-	-	0.002

†less than
(Sodium (Na) -- less than 0.19% in each)
*Analysis done by Anamet Laboratories, Berkeley, California

Table 5. Electron Microprobe Analysis for Al:Si Ratios(1)

Specimen	Results from computer processed data(2) Al:Si Ratio	Calculations from raw data(3) Al:Si Ratio	Data from Table 5 (4) wt/o
M1	1.5:1	2:1	Al Princ. Const. Si 18.7
M2	5:1	6:1	Al Princ. Const. Si 11.7
M3	2:3	5:6	Al 18.5 Si Princ. Const.
M4	1.9:3	4.8:6	Al 13.2 Si Princ. Const.

Notes:

(1) SiO_2 and Al_2O_3 standards

(2) Integrated Si and Al content of all phases

(3) Calculations exclude counts taken while scanning visible, distinctive particles

(4) Semi-quantitative spectrographic analysis

Table 6. Density and Porosity

	M1	M2	M3	M4
Bulk Density (g/cm^3)	3.204	3.351	3.079	3.082
Apparent Density (gm/cm^3)	3.209	3.354	3.081	3.082
Open Porosity (%)	0.191	0.090	0.049	0.007

Table 7. Coefficients of Thermal Expansion

M1:	$3.25 \times 10^{-6}/°C$
M2:	$2.85 \times 10^{-6}/°C$
M3:	$2.77 \times 10^{-6}/°C$
M4:	$2.96 \times 10^{-6}/°C$

Table 8. Relative Machining Difficulty (i.e., cutting of billets)*

Specimen type	Remarks
M1	Maximum of 0.005" depth of cut per pass; broke blade attempting 0.01" cut on slow first pass. With new blade, started at 0.001" depth of cut, gradually increasing to 0.005" for all subsequent cutting.
M2	Maximum of 0.002" depth of cut per pass in either direction (i.e., up-cut or down-cut - table movement versus blade rotation direction). Damaged blade when attempting 0.0025" depth of cut per pass in pressing direction after sawing nearly all specimens at 0.002" depth of cut.
M3	Maximum of 0.0015" depth of cut until through surface layer. Thereafter, used 0.0015" for down-cutting and 0.002" for up-cutting. In cutting perpendicular to specimen pressing direction, a depth of cut of 0.0025" could be used.
M4	Maximum of 0.002" depth of cut used per pass in either direction of table movement. Definitely easier to cut in pressing direction, or perpendicular to it, than M3, although surface hardness noticed in cutting M3 was also present in M4. A more rapid table movement could be made with no apparent extra strain on blade than in cutting M3.

* High speed precision grinder (19,000 rpm) with 0.010" D220 grit MA 1/16" diamond blade.

Table 9. Microhardness
(Vickers - 1000g load)

Specimen	VHN
M1	955 - 1300
M2	1430
M3	1470 - 1330
M4	1525 - 1600

Note: Coe, Lumby, and Dawson, for hot-pressed Si_3N_4, found that microhardness decreased with load on the tester (see ref. 33)

Table 10: Results of Compressive Testing at High Temperature
(Applied strain rate of 1×10^{-5} s^{-1})

Specimen	Temperature °C	Elastic Limit ksi	Yield Stress @ 0.2% strain ksi	Maximum Stress ksi	Strain at Max. Stress %
M1	1200	55.1	70.5	79.1	3.95
	1300	32.8	63.2	66.0	3.00
	1400	13.6	20.3	23.8	3.25
M2	1200	74.3	91.8	112.2	5.50
	1300	76.6	94.9	115.9	4.55
	1400	76.8	89.0	98.4	5.30
	1500	13.4	16.8	18.7	3.20
M3	1200	80.0	94.4	94.7	3.80
	1300	63.1	78.0	84.6	4.67
	1400	16.2	44.6	50.5	5.50
M4	1200	70.9	88.7	105.0	5.60
	1300	63.5	80.1	84.8	4.47
	1400	21.1	37.5	50.9	5.75

Table 11: Bending Strength in as-received condition and after thermal shock at 400 °C

Room Temperature	4-Point Bend Strength (ksi) (Loading rate: 0.0005"/min)			
	M1	M2	M3	M4
As Received (square cross-section)	35.8*	43.6	20.0	25.0
As Received (rectangular cross-section)		41.0	31.0 23.0	25.4 24.6
After thermal shock @ 400 °C (rectangular cross-section only)	8.9 19.2†	18.4** 8.0**	11.4 13.7	20.0

* Loading rate was 0.0002"/min
† Thermally shocked @ 1000 °C
** Data furnished by P. C. Dokko

Table 12: Oxidation - Weight gain after 3 hr in air at 1400 °C

Specimen	weight gain mg/cm^2*
M1	3.0
M2	8.3
M3	0.6
M4	0.17

*Computed on basis of nominal sized specimen (0.1 x 0.1 x 0.3 in.)

Table 13. Corrosion - Weight Loss after 4 hours and 24 hours in 16% HF solution.

4 hours

Specimen	Weight Loss (grams)	Weight Loss (%)
M1	0.251	14.0
M2	0.0238	1.3
M3	0.649	23.3
M4	0.459	21.3

24 hours

Specimen	Weight Loss (grams)	Weight Loss (%)
M1	0.718	40.0
M2	0.180	9.4
M3	2.210	79.2
M4	1.667	77.4

Table 14. Results Overview.

1. Structure type:

   M1 -- Mixture of β^1-Si_3N_4, 15R-AlN polytype, α-Al_2O_3

   M2 -- 15R-AlN polytype, formula
   $Si_{(1.1 \text{ to } 0.4)}Al_{(3.5 \text{ to } 2.5)}O_{(1.2 \text{ to } 2)}N_{(3.2 \text{ to } 2.7)}$

   M3)
   M4) -- β^1-Si_3N_4, formula: $Si_{6-x}Al_xO_xN_{8-x}$

		Highest		Lowest	
2. Densities		M2	M1	M4	M3
3. Open porosities		M1	M2	M3	M4
4. Thermal expansion		M1	M4	M2	M3
5. Microhardness		M3	M4	M2	M1
6. Machining difficulty		M3	M4	M2	M1
7. Oxidation resistance		M4	M3	M1	M2
8. Corrosion resistance		M2	M1	M4	M3
9. Compressive strength	(1400°C)	M2	M4	M3	M1
	(1300°C)	M2	M4	M3	M1
	(1200°C)	M2	M4	M3	M1
10. Bend strength (r.t.)		M2	M1	M4	M3
11. Thermal shock resistance		M4	M2	M3	M1

FIGURE CAPTIONS

Figure 1: Basic Si_3N_4 tetrahedron

Figure 2: Crystal structure of β-Si_3N_4

Figure 3: Basal plane of α- and β-Si_3N_4 (after Thompson and Pratt[14])

Figure 4: Atomic arrangement in β-Si_3N_4 (after Wild, Grieveson, and Jack[15].

Figure 5: Atomic arrangement in α-Si_3N_4 (after Wild, Grieveson, and Jack[15])

Figure 6: Approximate phase diagram for the system Si_3N_4-AlN-Al_2O_3 at 1730 °C, (after Oyama[17])

Figure 7: System Si-Al-O-N: the subsection Si_3N_4-AlN-$Al_2)_3$-SiO_2 is a square plane. (After Gauckler, Lukas, and Petzow[21]^2

Figure 8: Isothermal section Si_3N_4-AlN-Al_2O_3-SiO_2 of the system Si-Al-O-N at 1760 °C. (Dashed lines are tentative for a temperature slightly below 1760 °C). (After Gauckler, Lukas, and Petzow (21)).

Figure 9: Arrangement for compressive tests.

Figure 10: Arrangement for bend tests.

Figure 11: X-ray diffraction of materials as-received.

Figure 12: Materials in as-received condition, 500X; polished, no etch; cross polarized light; A: M1, B: M2, C: M3, D: M4.

Figure 13: Microstructure of materials in as-received, polished condition, 800X, 3 min HF etch; A: M1, B: M2, C: M3, D: M4.

Figure 14: Scanning electron micrographs of rod-like particles in microstructure; as-received, polished, 1 min HF etch, 10,000X. A: M1, B: M2, C: M3, D: M4.

Figure 15: Scanning electron micrographs of M1 material, as received, polished, 10 sec HF etch. A: 1000X, B: 10,000X, C: EDAX peaks (L to R -Al, Si, Ca, Ti, Mn, and Fe (Kα and Kβ), D: EDAX shows primarily Al and Fe (Kα and Kβ) for light spot in center of B.

Figure 16: Scanning electron micrograph of M1 material as-received, polished, 3 min HF etch, 500X.

Figure 17: Thermal expansion by dilatometric at 2°C per minute heating rate.

Figure 18: Stress-strain curves for applied strain rate of $1 \times 10^{-5} s^{-1}$ at 1200 °C.

Figure 19: Stress-strain curves for applied strain rate of $1 \times 10^{-5} s^{-1}$ at 1300 °C.

Figure 20: Stress-strain curves for applied strain rate of $1 \times 10^{-5} s^{-1}$ at 1400 °C.

Figure 21: Stress-strain curve for applied strain rate of $1 \times 10^{-5} s^{-1}$ at 1500 °C.

Figure 22: Variation with temperature of yield stress at 0.2% offset strain, in compression.

Figure 23: Scanning electron micrograph of fracture surface of M1 tested at 1200 °C, 500X.

Figure 24: Scanning electron micrograph of interior of M1 after fracture at 1200 °C, 5000X.

Figure 25: Result of compression testing of M1 material at 1400 °C. (A and C are optical photomicrographs; B and D are scanning electron micrographs. A: Exterior view showing barrelling and surface layer, 10X, B: Sectional view showing external layer, 500X, C: Edge of specimen viewed under cross-polarized light, 500X, D: Interior, 2000X.

Figure 26: Scanning electron micrographs of microstructures of M2 material after compressive testing, 2000X. A: 1200 °C, B: 1300 °C, C: 1400 °C.

Figure 27: Scanning electron micrographs of interior sections of M3 and M4 materials after compressive testing, 2000X. A: M3 at 1300 °C, B: M3 at 1400 °C, C: M4 at 1300 °C, D: M4 at 1400 °C.

Figure 28: Scanning electron micrograph of M3 specimen fractured in R.T. 4-point bending, 50X. Tensile surfaces are at the top in photographs. Lower photograph is enlargement of upper left-hand corner as viewed at top.

Figure 29: Scanning electron micrograph of R.T. fracture surface of M4 specimen, 100X. Tensile surface is at the top of the photograph.

Figure 30: Scanning electron micrograph of R.T. fracture surface of M3 specimen after thermal shock, 50X. Tensile surface is at the top of the photograph as viewed.

Figure 31: Scanning electron micrograph of an M4 specimen, viewed from above, thermally shocked then bend-tested at room temperature, 20X. Tensile surface is at left as viewed.

Areas marked 1, 2, and 3 are considered to be areas of slow crack growth.

Figure 32: Scanning electron micrographs of oxidized surfaces after heating in air for 3 hours at 1400 °C, 200X. A: M1, B: M2, C: M3, D: M4.

Figure 33: Weight loss versus time, exposure to acid (immersion in agitated 16% HF solution).

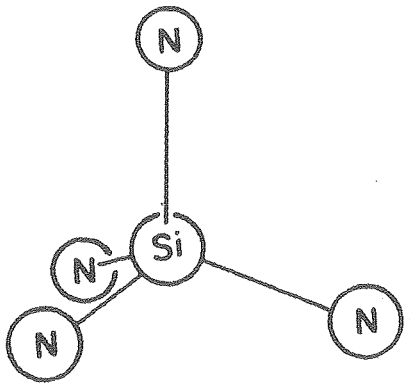

Fig. 1

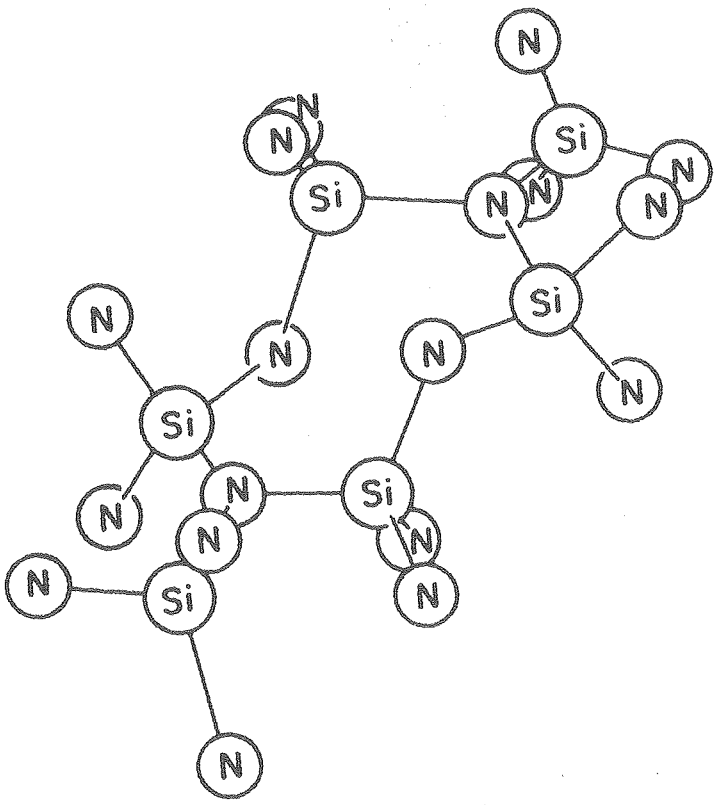

XBL 776-5581

Fig. 2

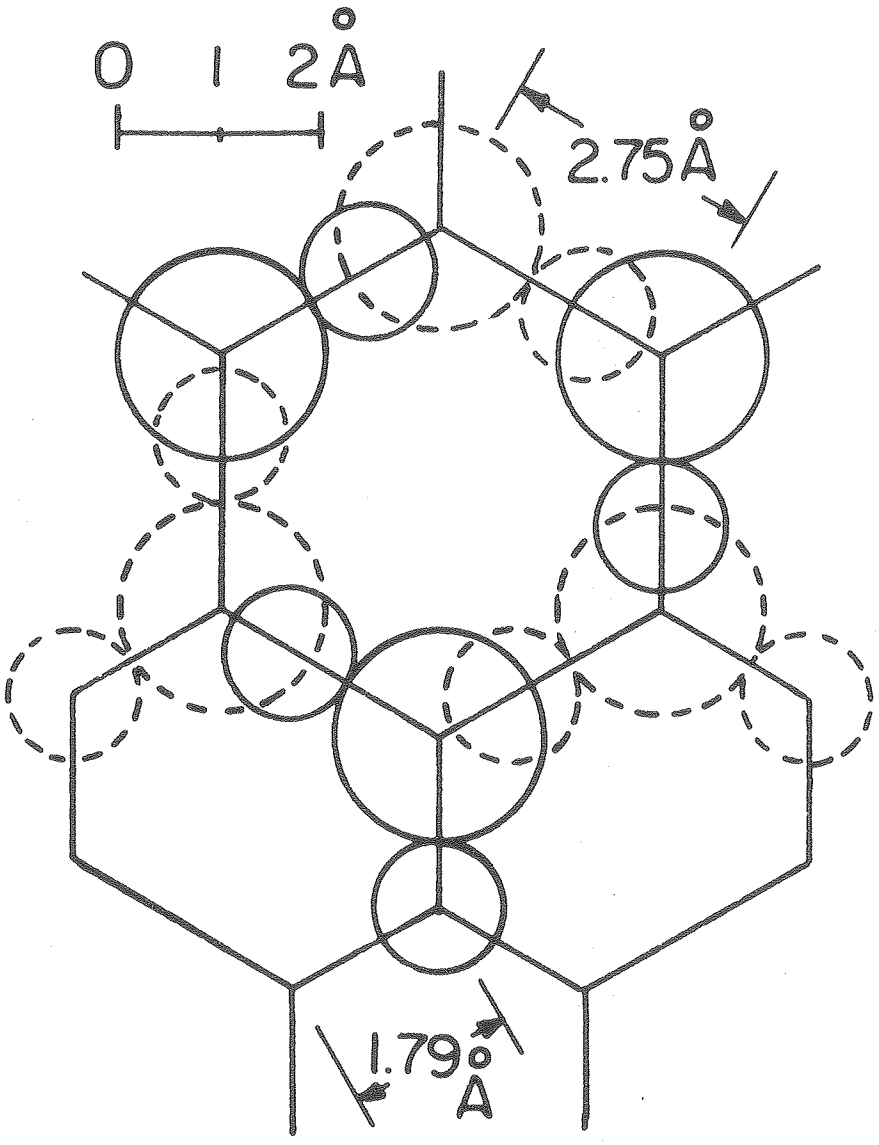

XBL 776 5582

Fig. 3

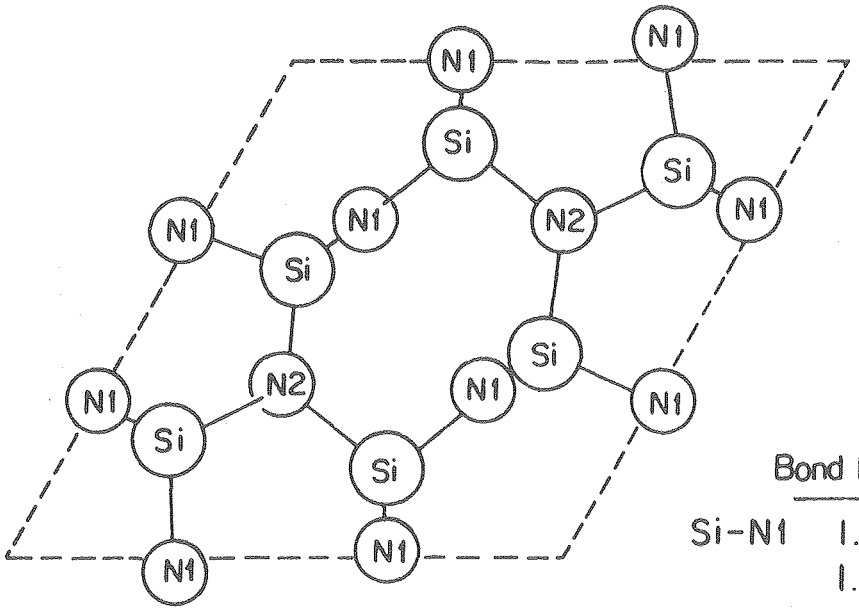

Fig. 4

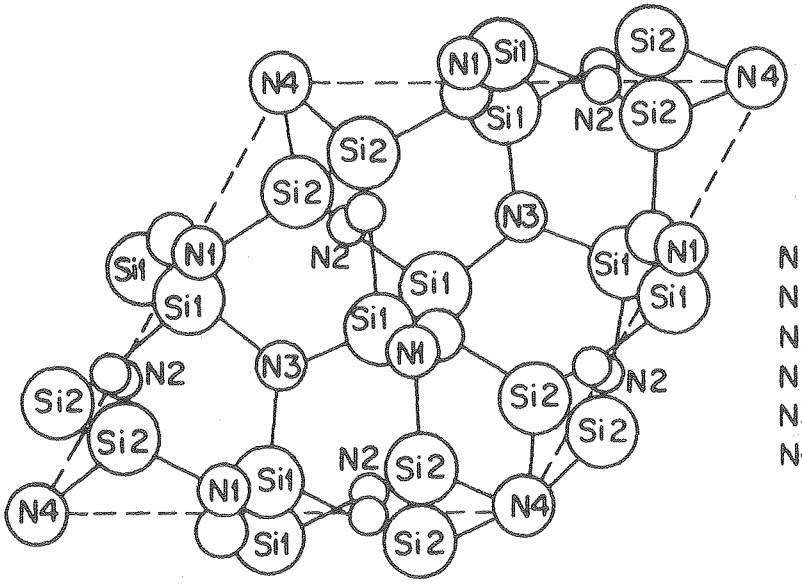

Bond Lengths (Å)

N1-Si1	1.566, 1.687
N1-Si2	1.896
N2-Si2	1.893, 1.562
N2-Si1	1.795
N3-Si1	1.781
N4-Si2	1.782

Fractional Heights, z

Si1	0.146, 0.646
Si2	0.451, 0.951
N1	0.400, 0.900
N2	0.115, 0.615
N4	0.384, 0.884

XBL 776-5584

Fig. 5

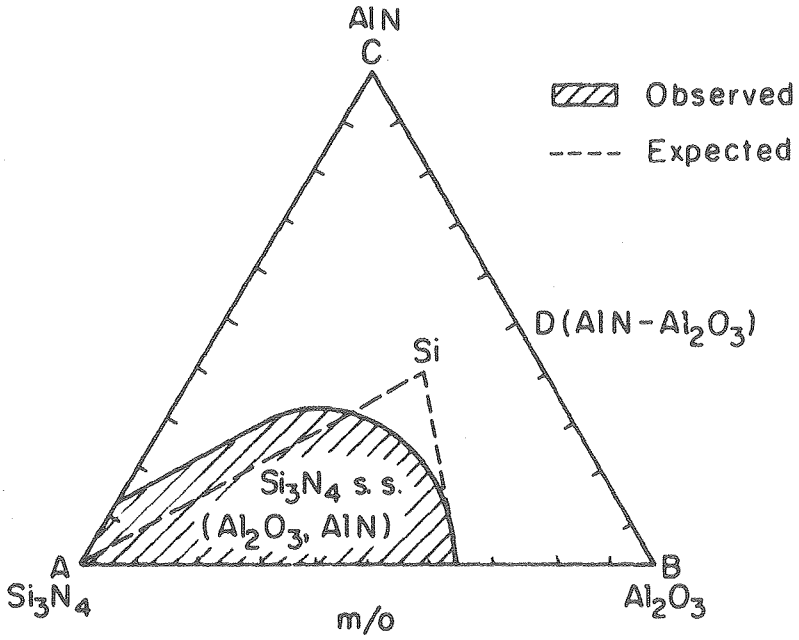

XBL 776-5585

Fig. 6

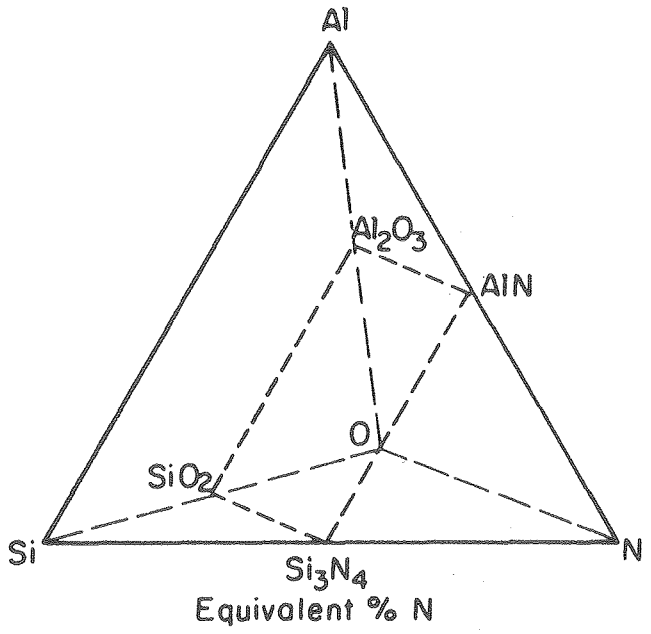

XBL 776-5586

Fig. 7

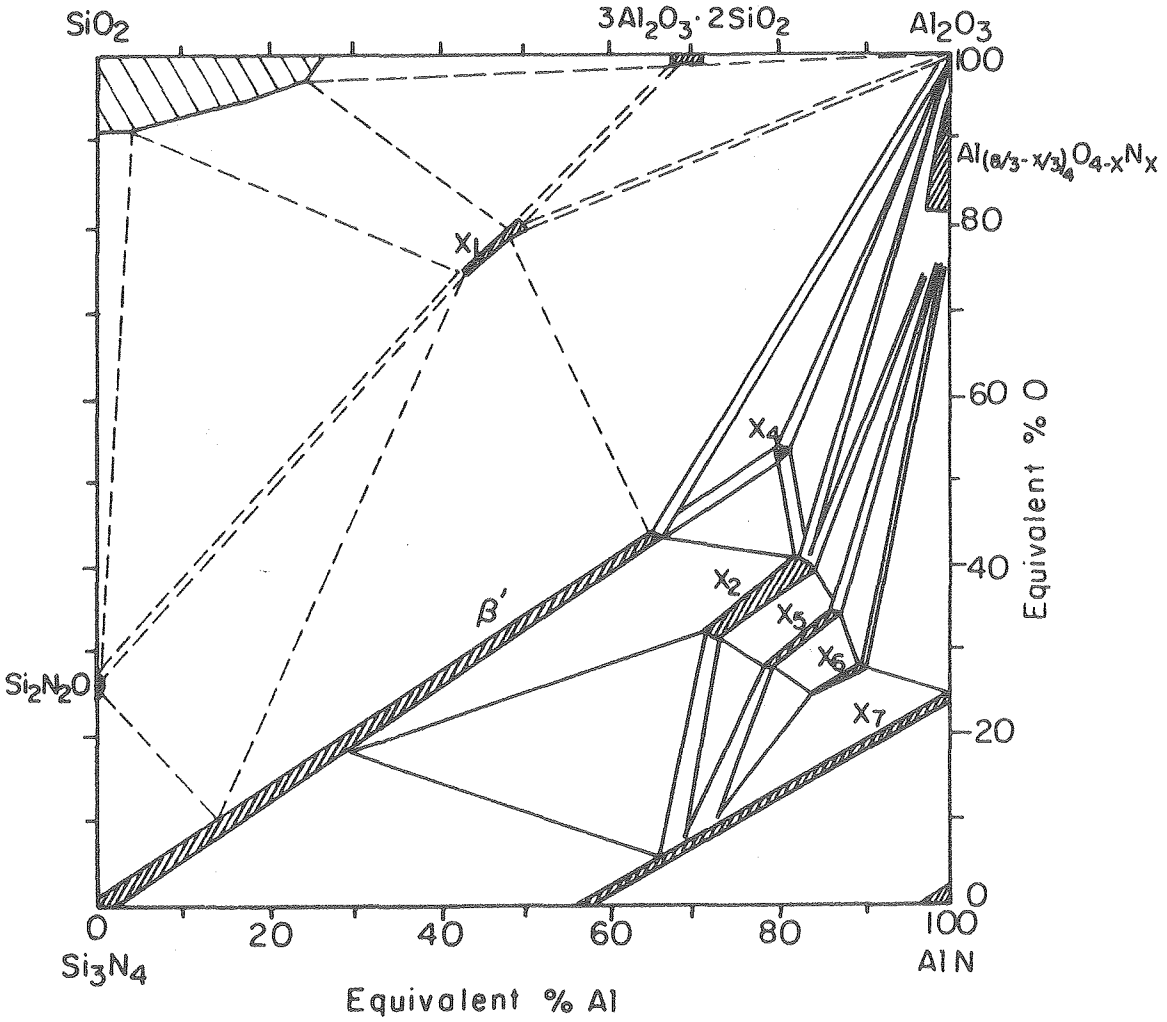

XBL 776-5587

Fig. 8

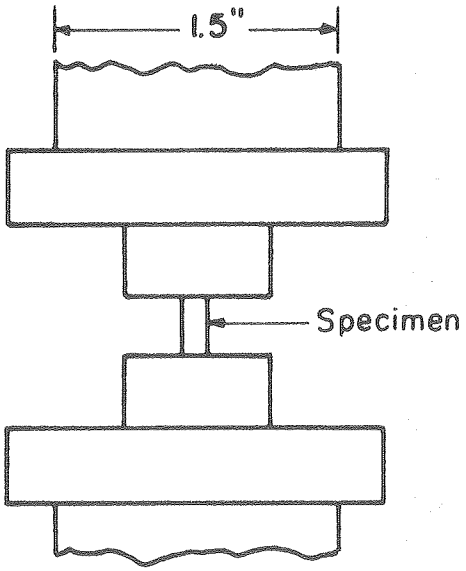

Fig. 9

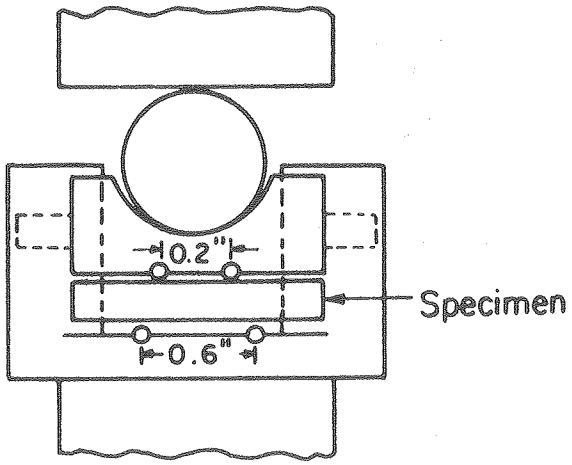

XBL 776-5588

Fig. 10

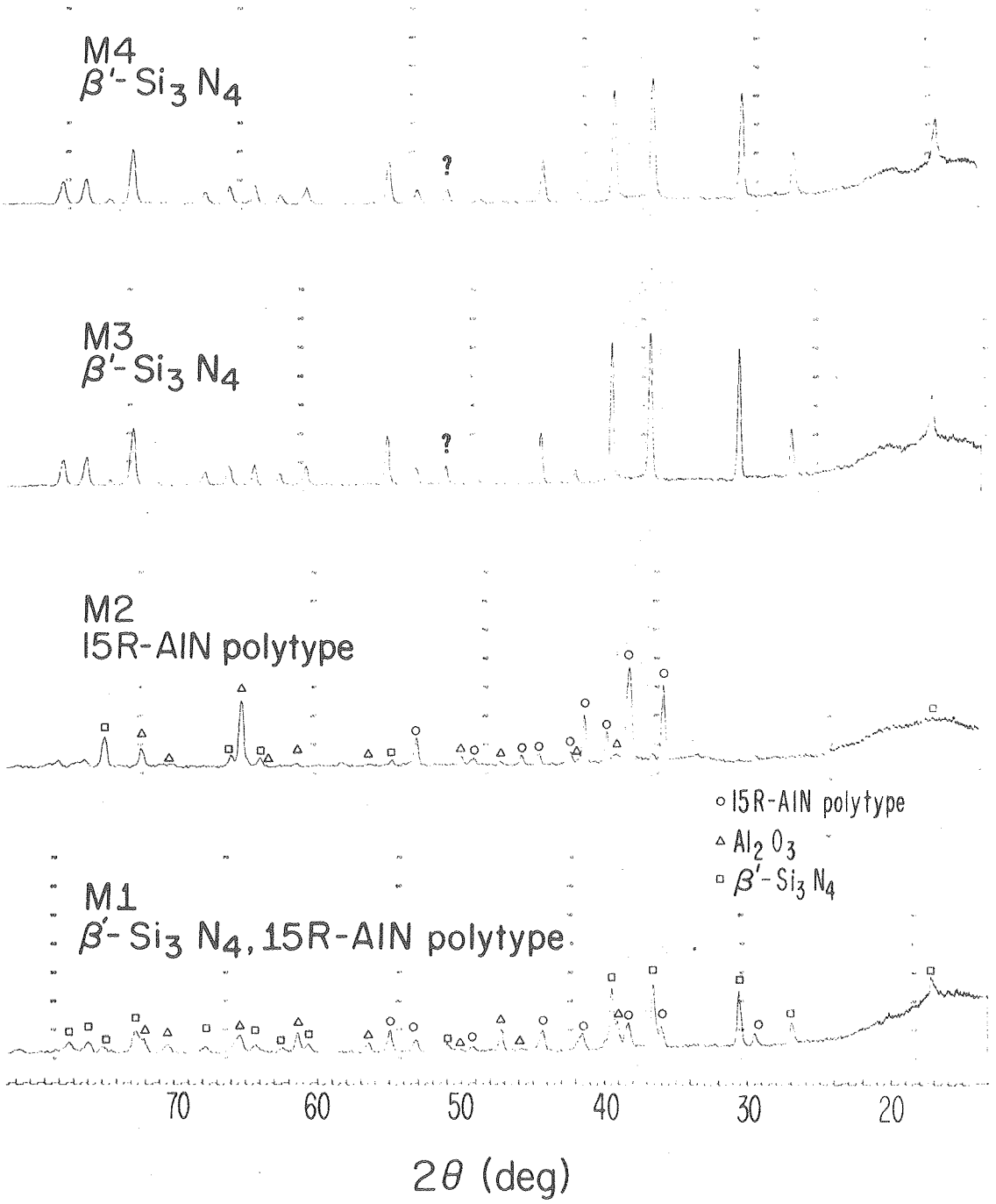

Fig. 11

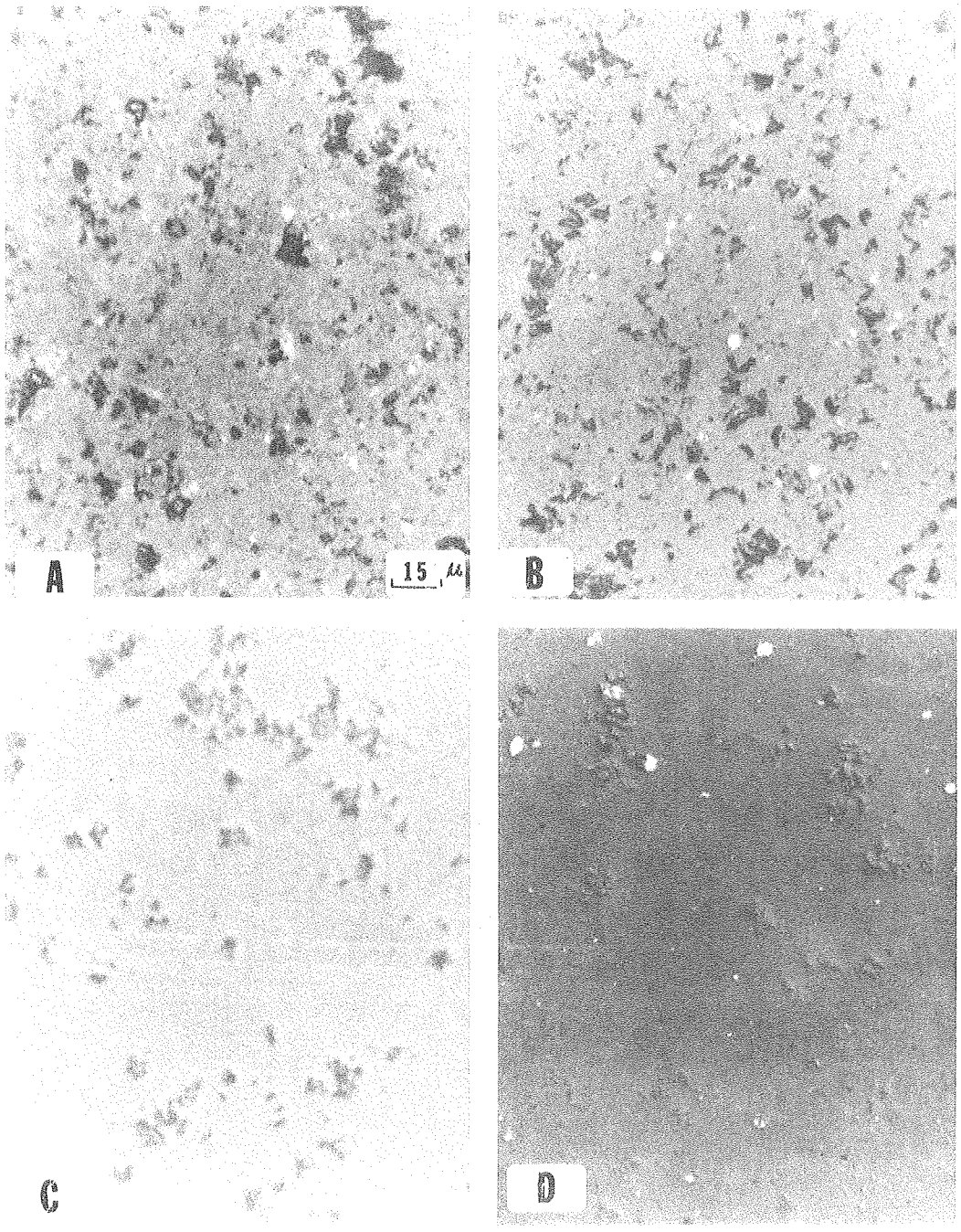

XBB776-5458

Fig. 12

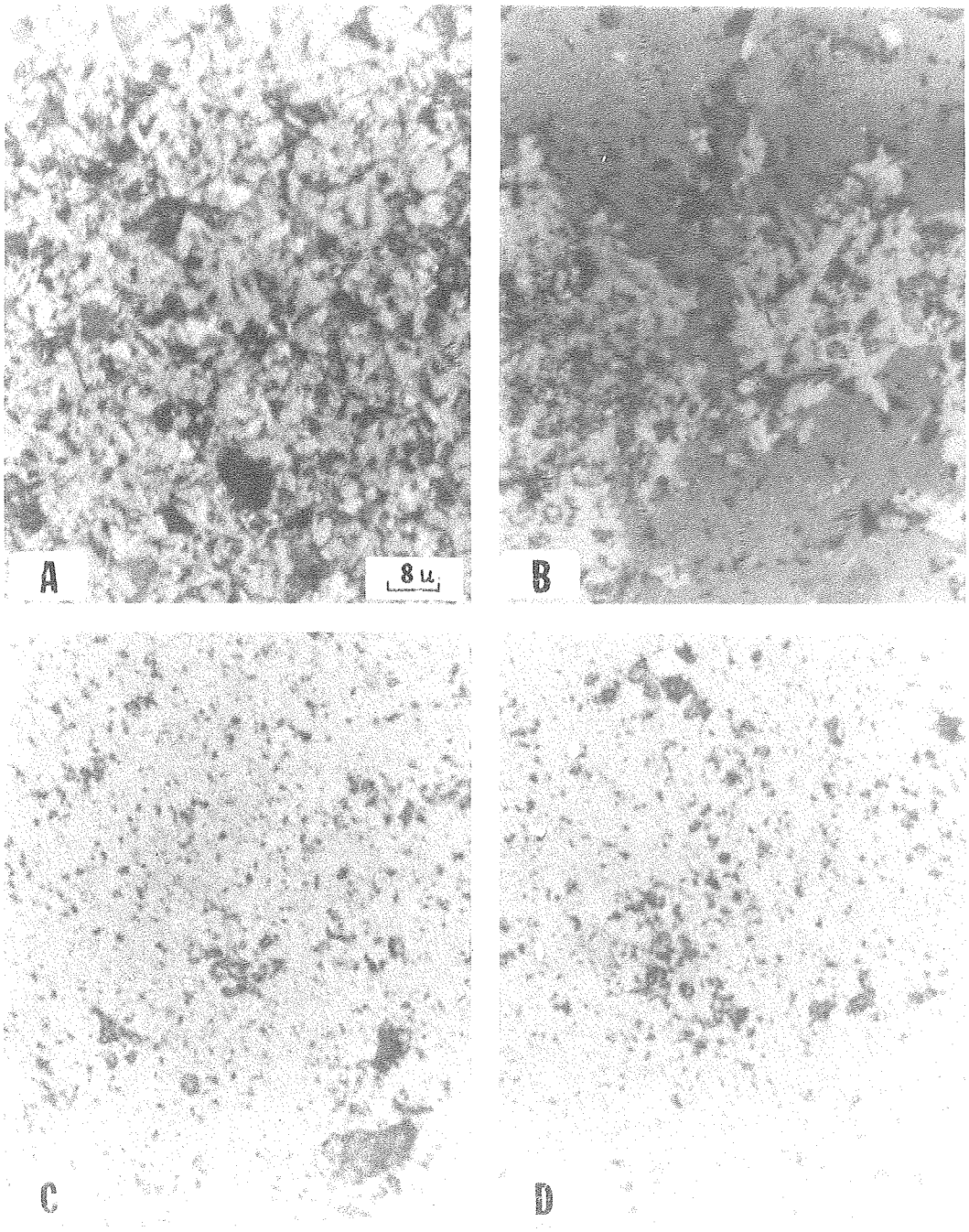

XBB776-5456

Fig. 13

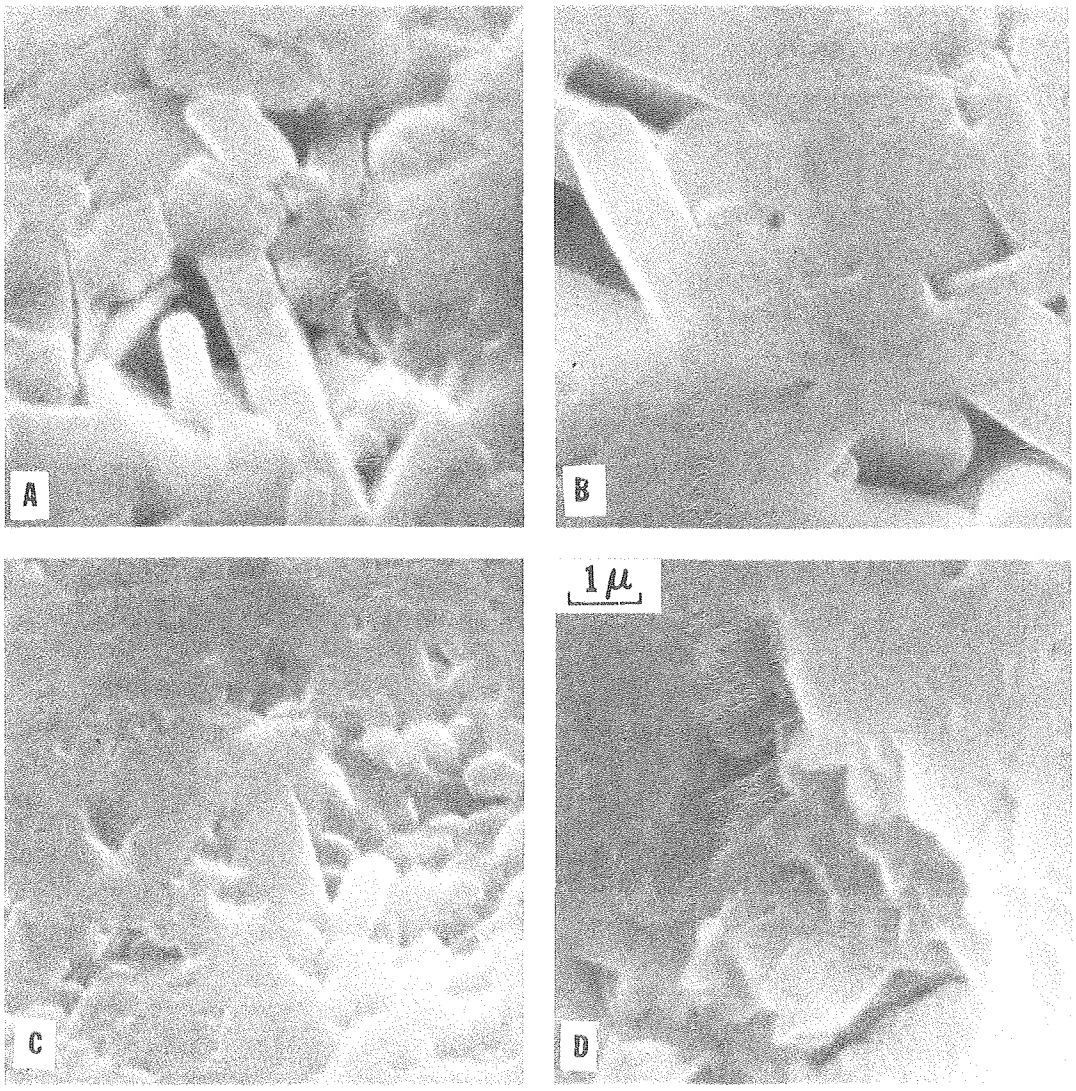

XBB776-5457

Fig. 14

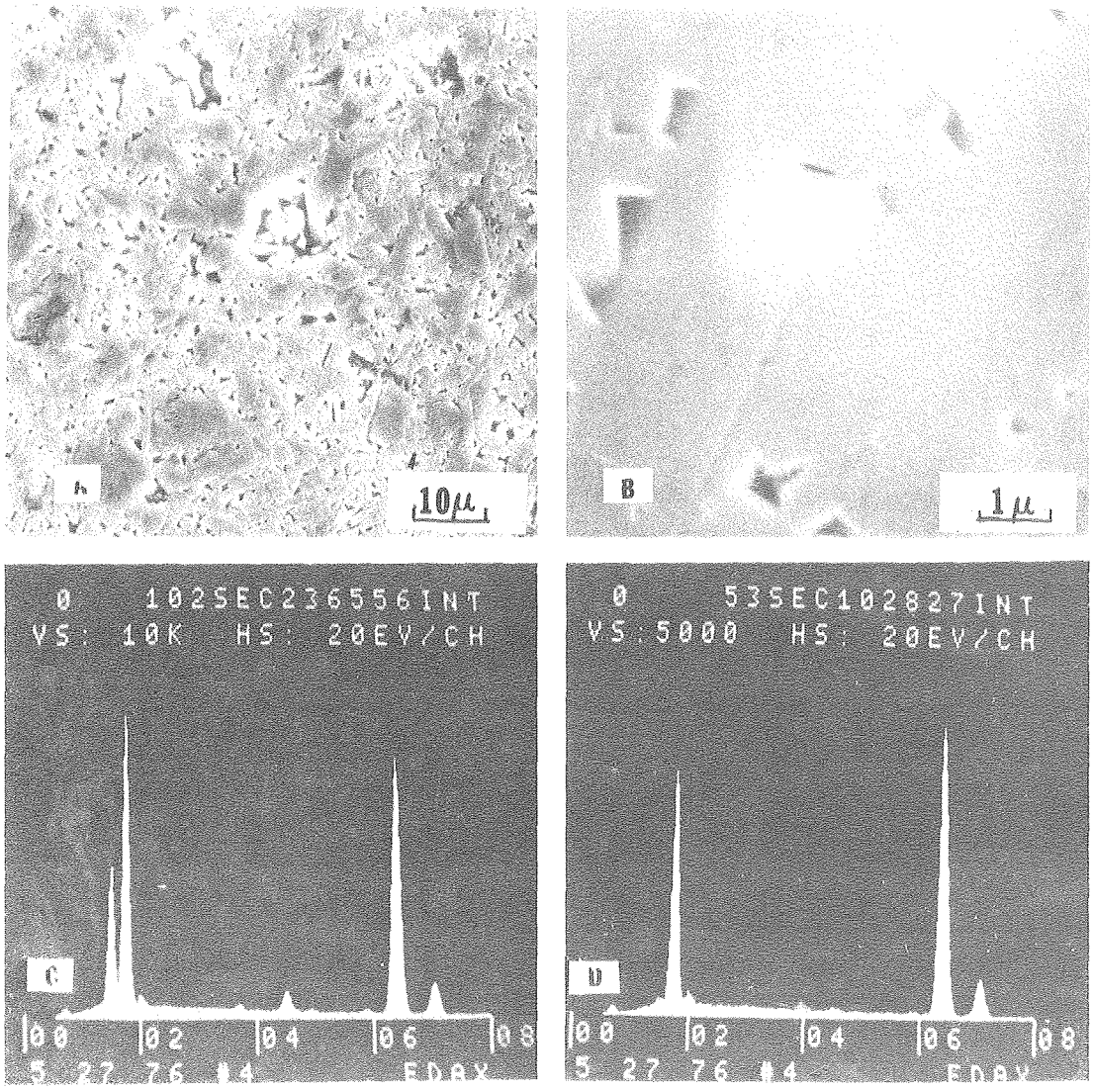

XBB776-5446

Fig. 15

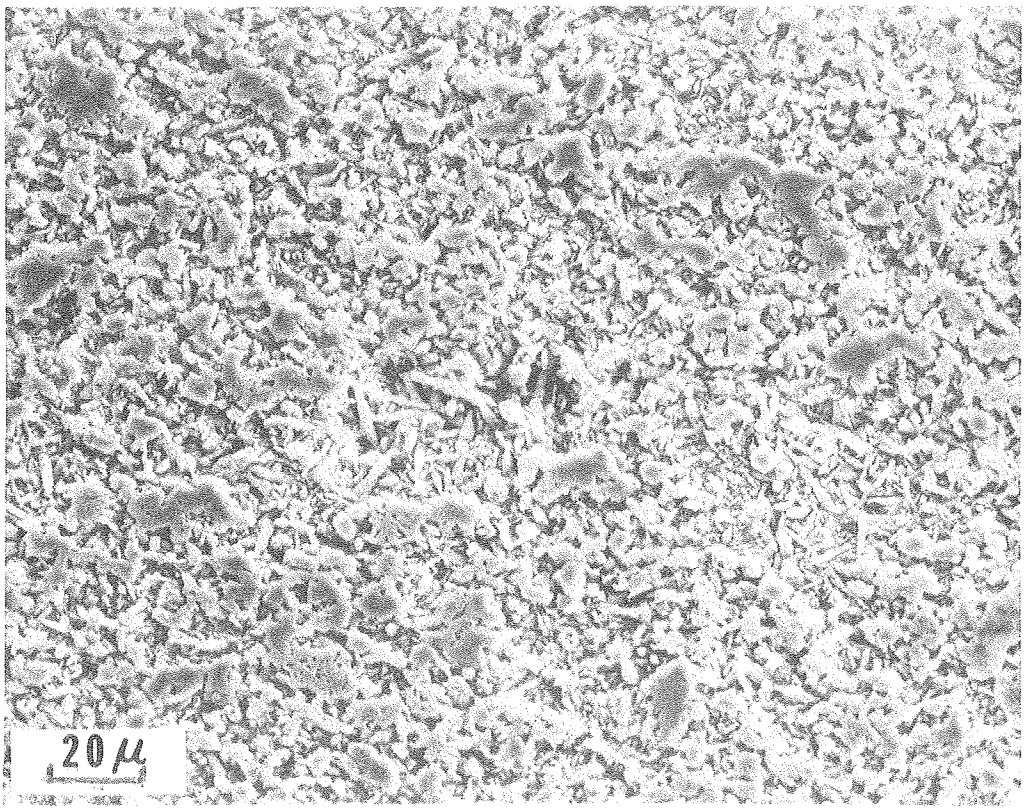

XBB776-5447

Fig. 16

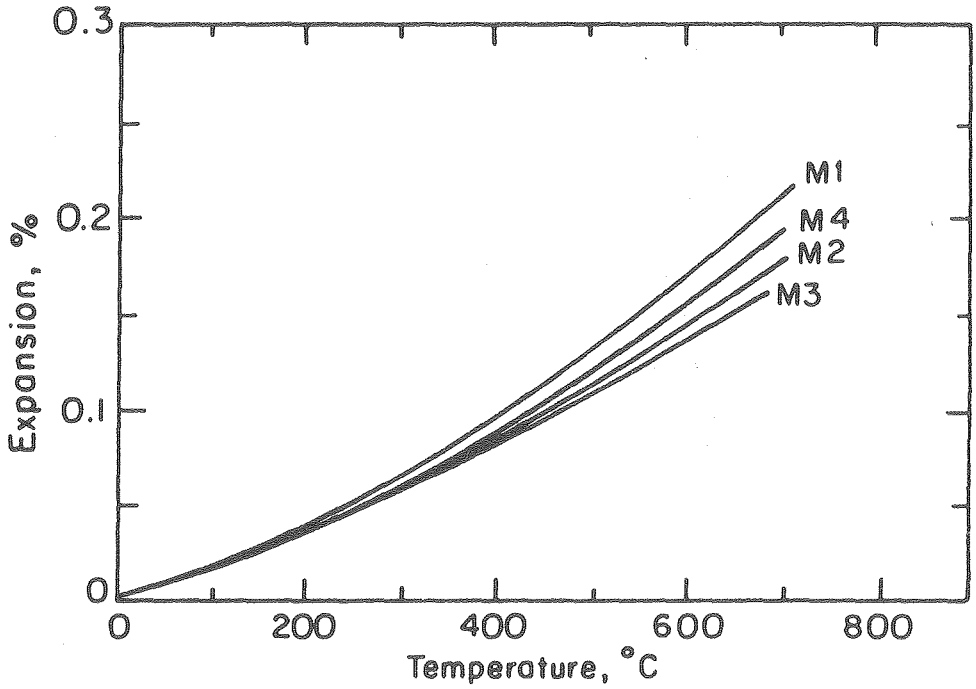

XBL 776-5589

Fig. 17

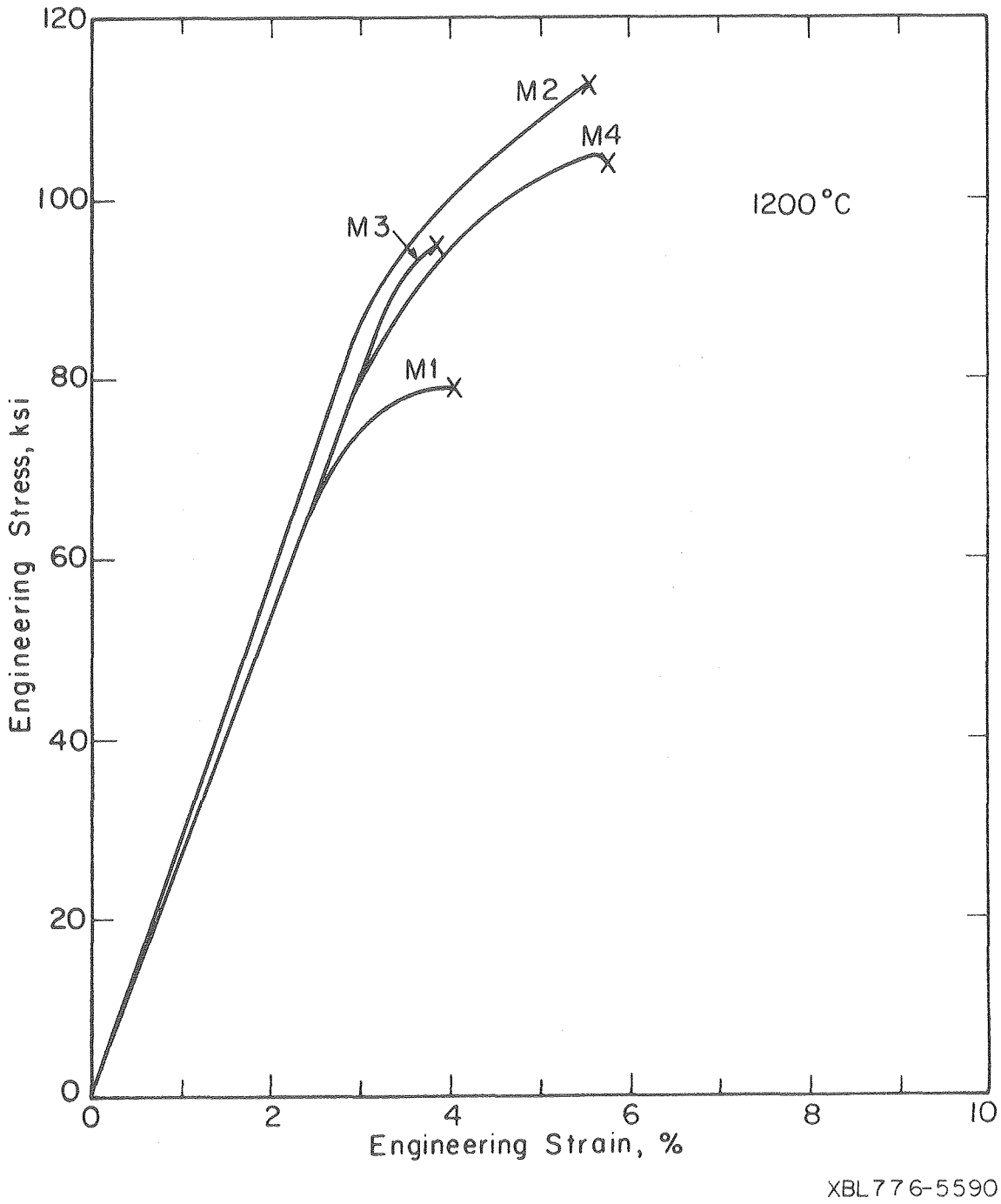
120
100
80
60
40
20
0
0
2
4
6
8
10
Engineering Stress, ksi
Engineering Strain, %
M1
M2
M3
M4
1200°C
XBL776-5590

Fig. 18

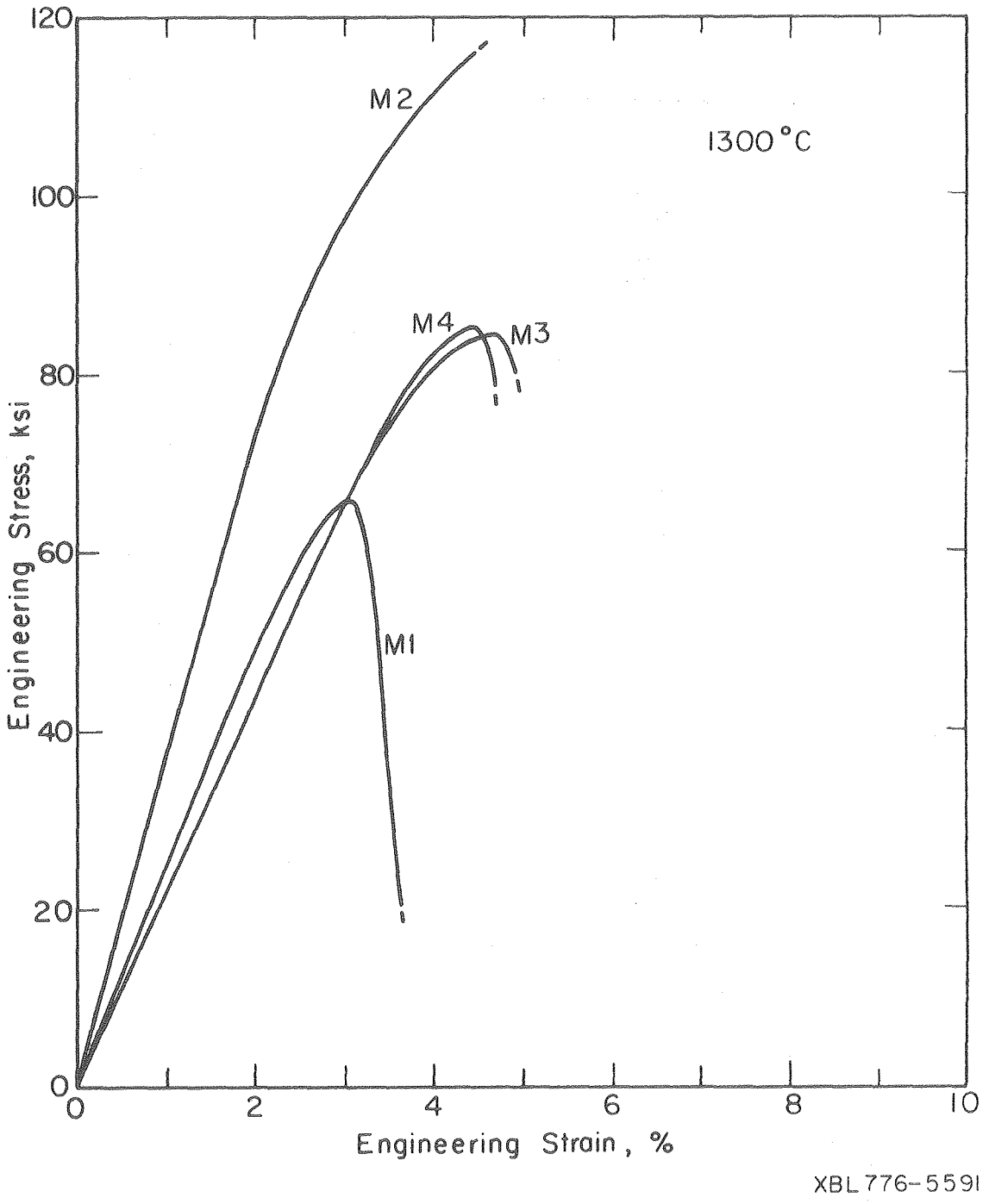

Fig. 19

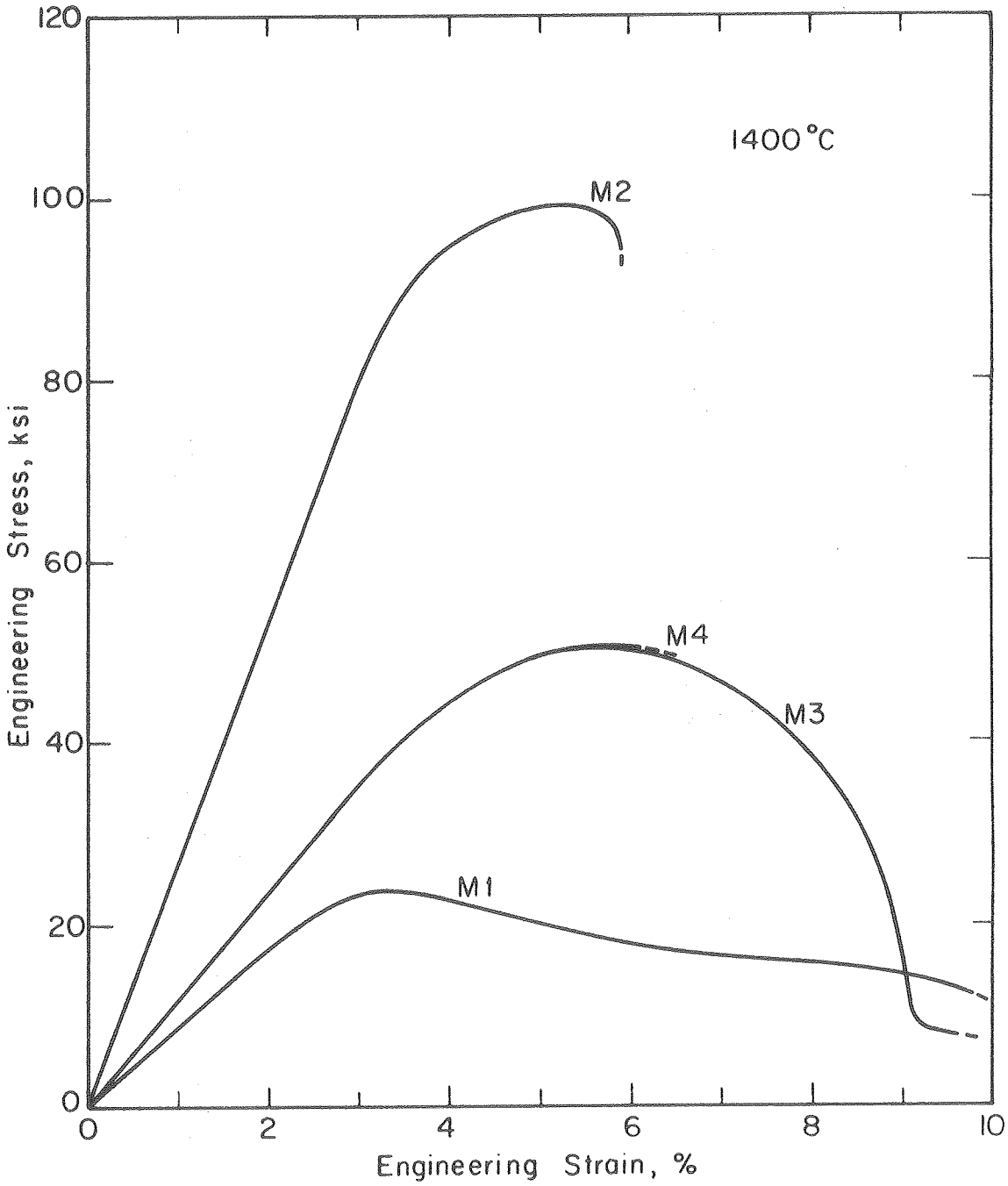

Fig. 20 Stress-strain curves for applied strain rate of 1 x $10^{-5}s^{-1}$ at 1400°C XBL 776-5592

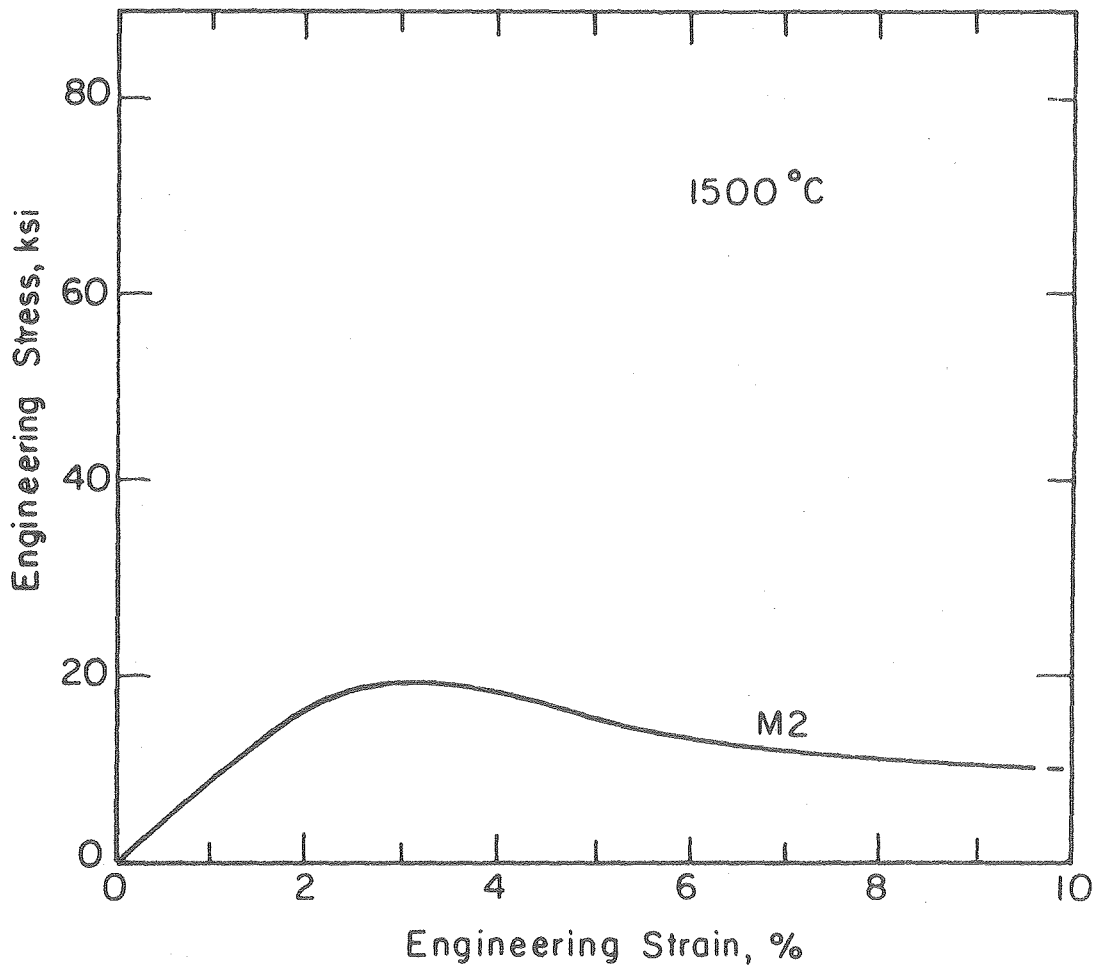

Fig. 21

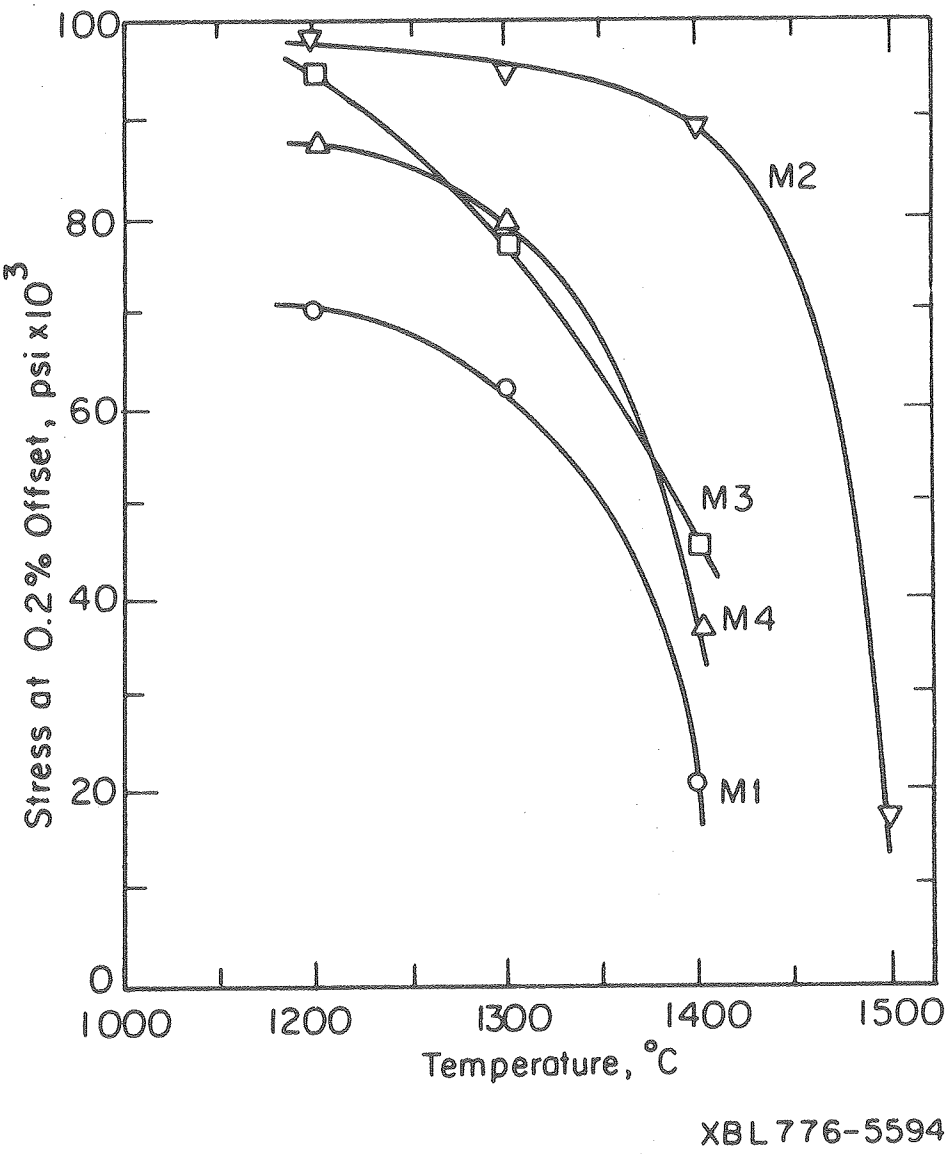
100
80
60
40
20
0
Stress at 0.2% Offset, psi x10^3
1000
1200
1300
1400
1500
Temperature, °C
M2
M3
M4
M1
XBL776-5594

Fig. 22

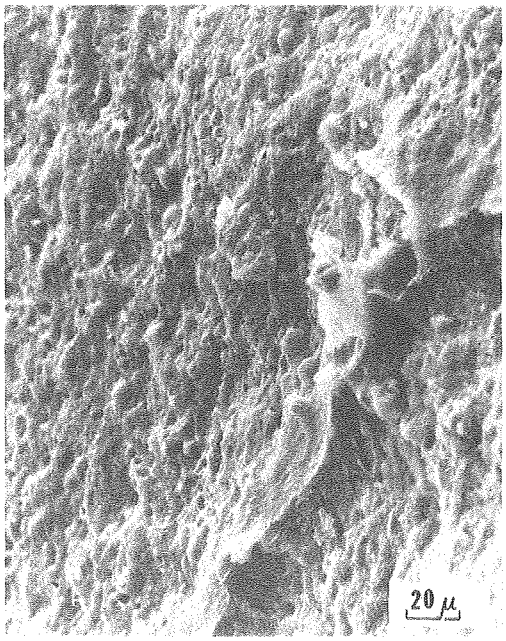

Fig.23

XBB776-5453

Fig. 24

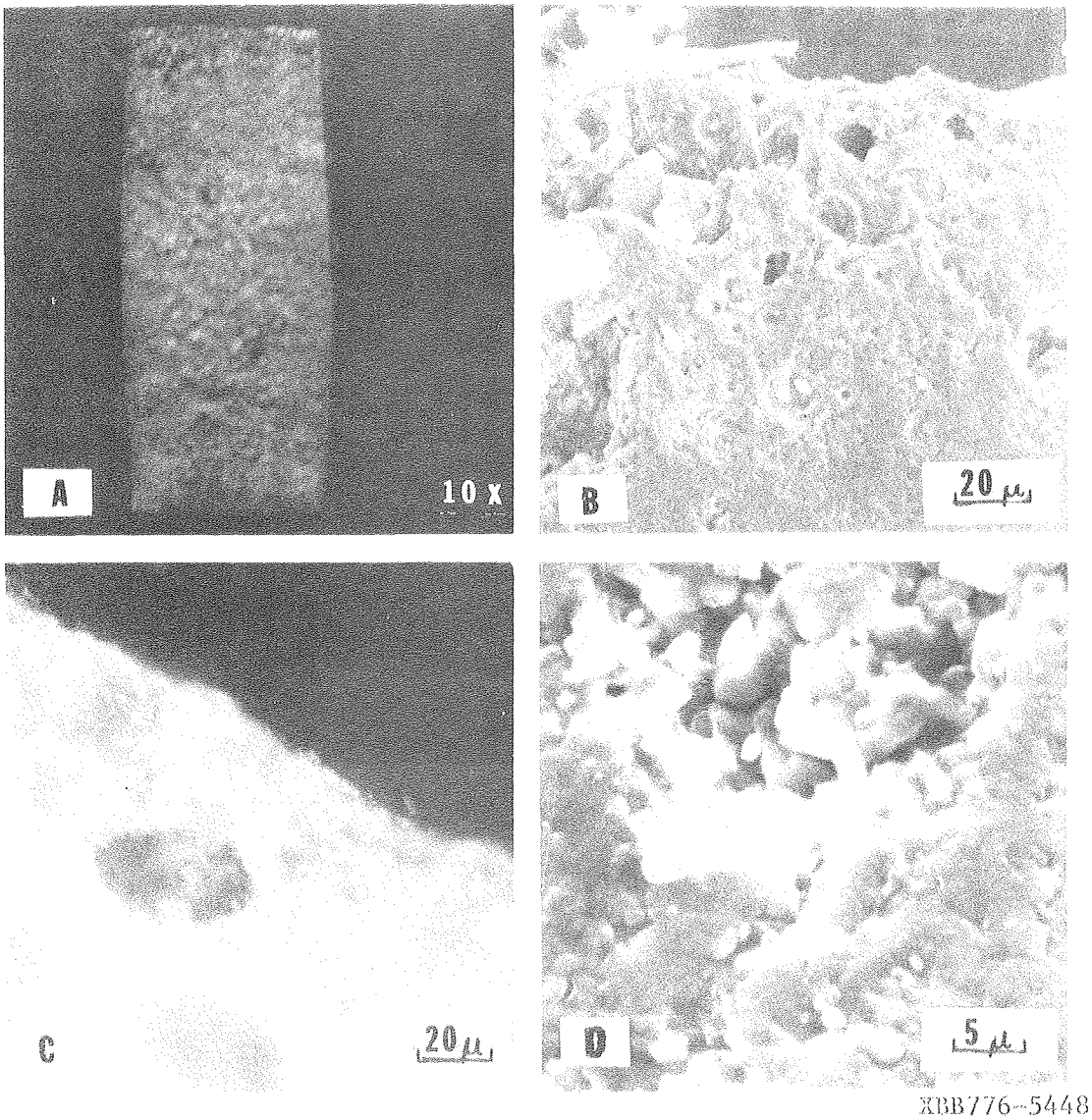

XBB776-5448

Fig. 25

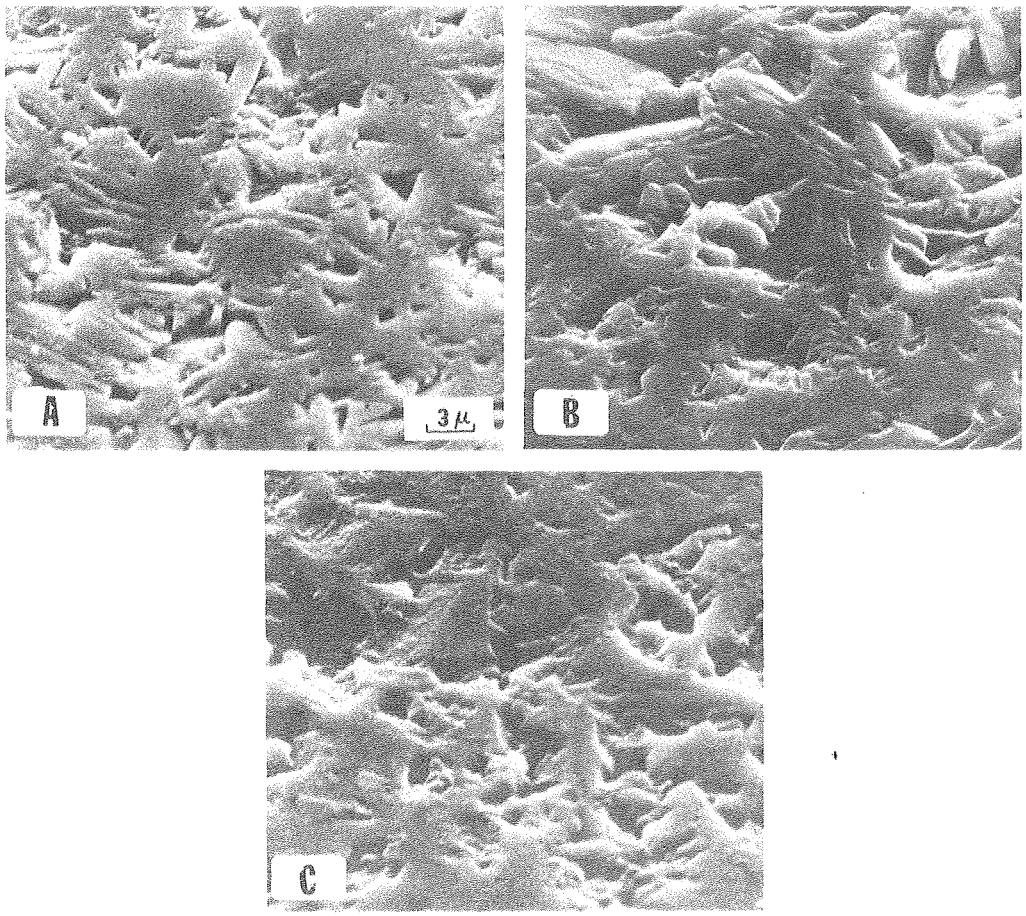

XBB776-5455

Fig. 26

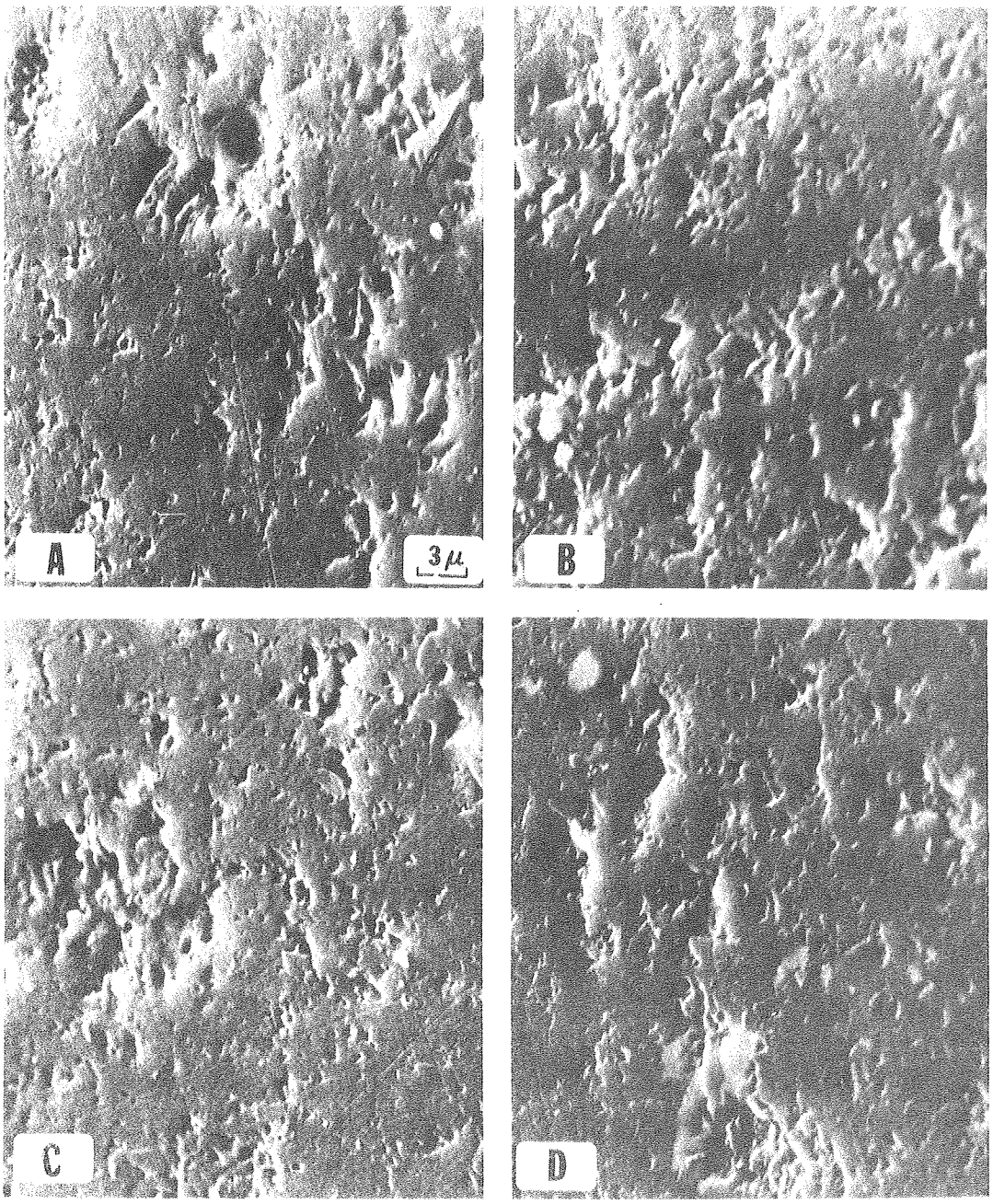

XBB776-5459

Fig. 27

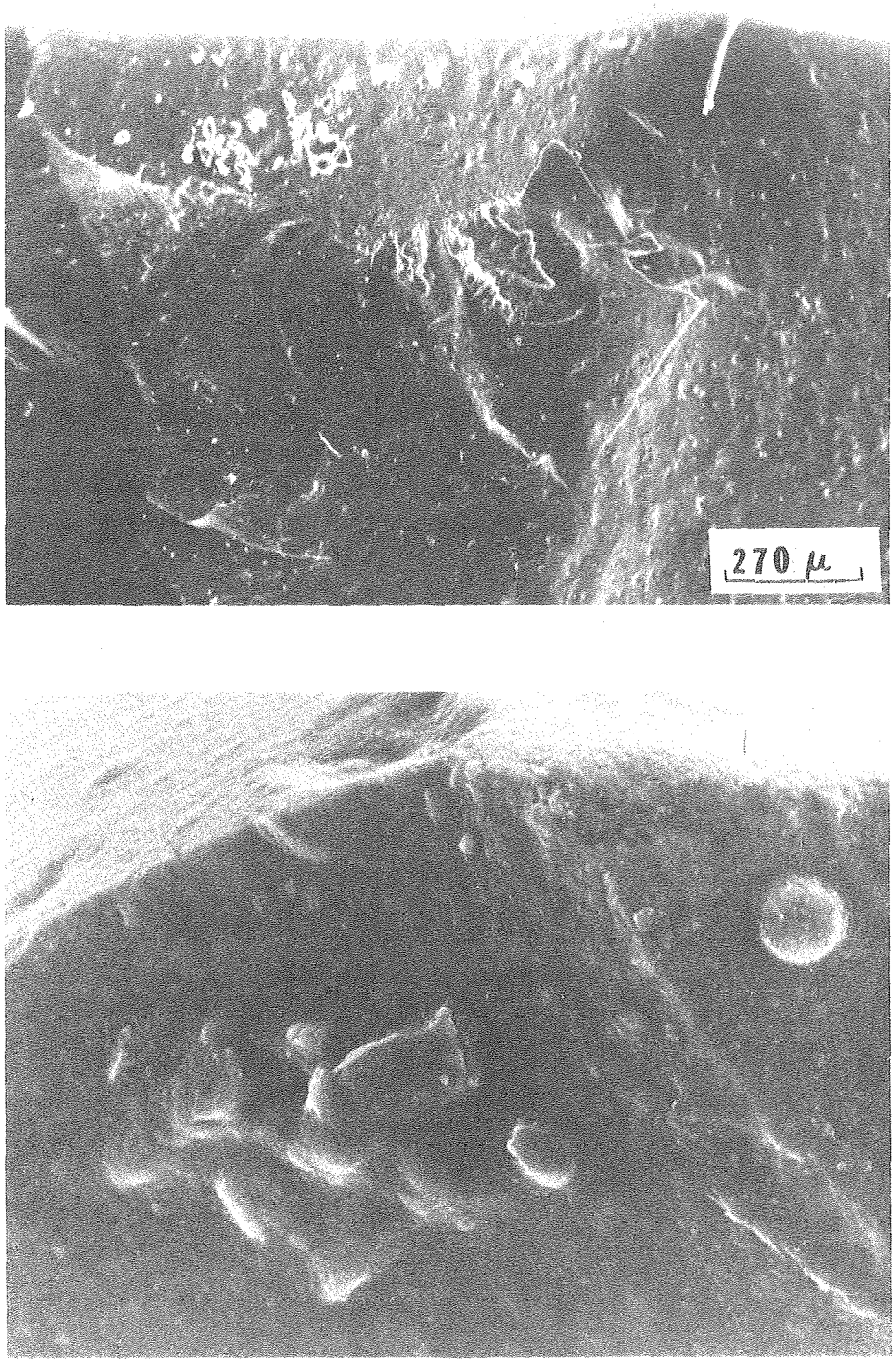

XBB776-5454

Fig. 28

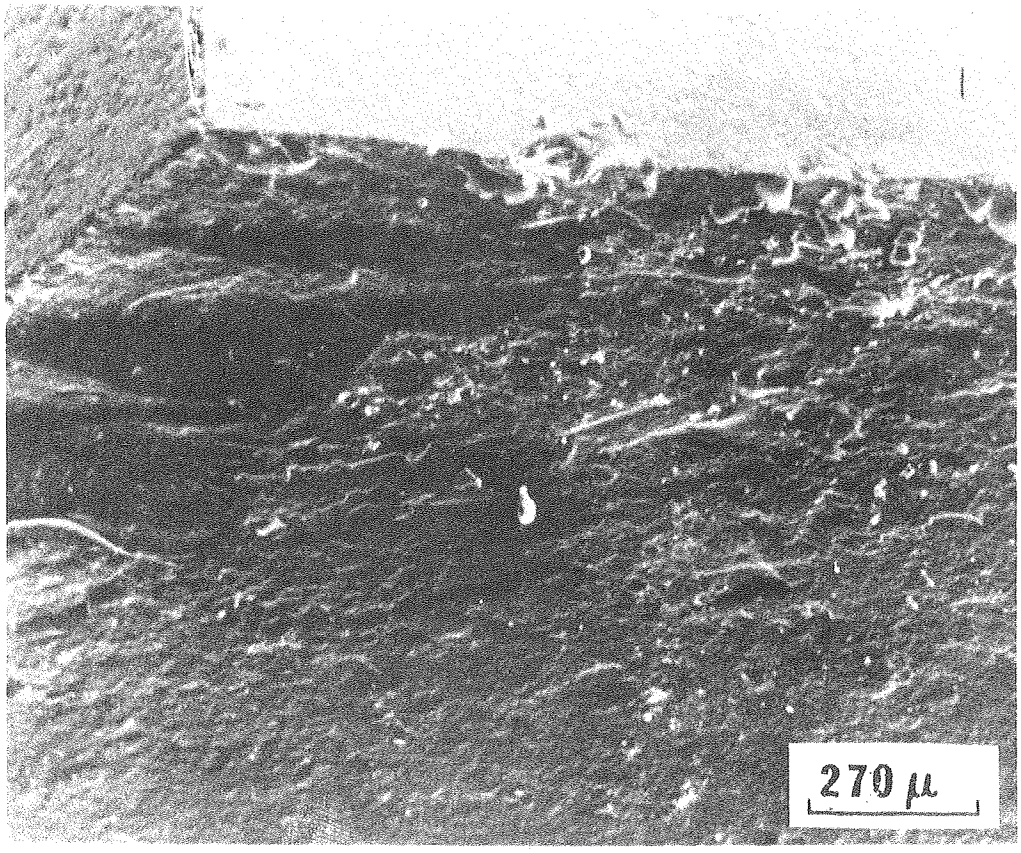

XBB776-5451

Fig. 29

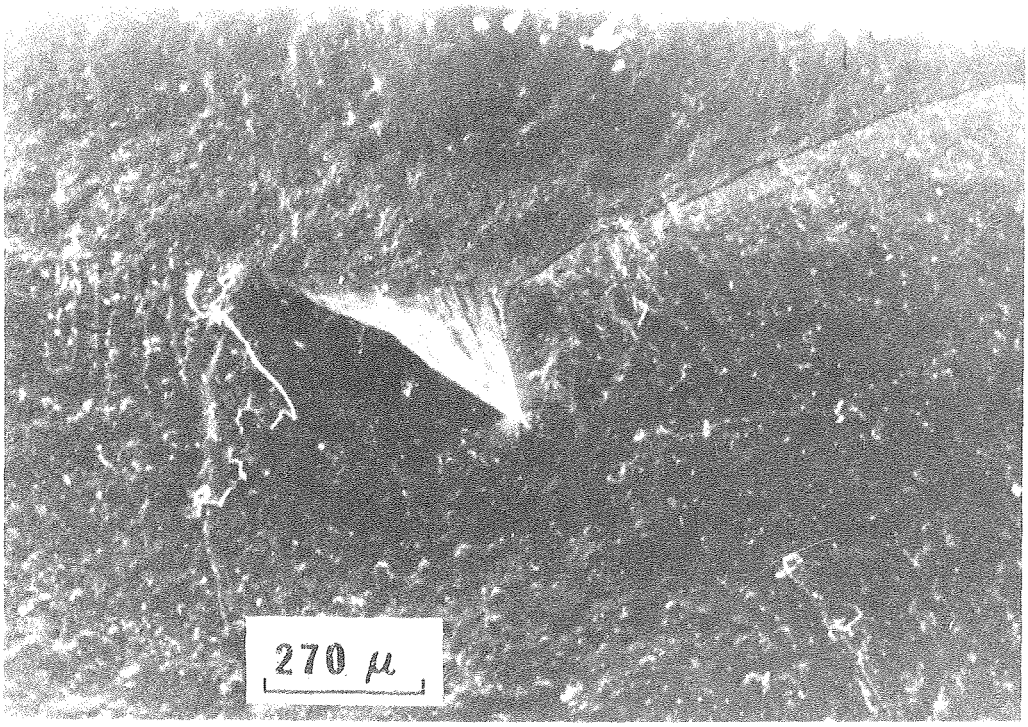

XBB776-5450

Fig. 30

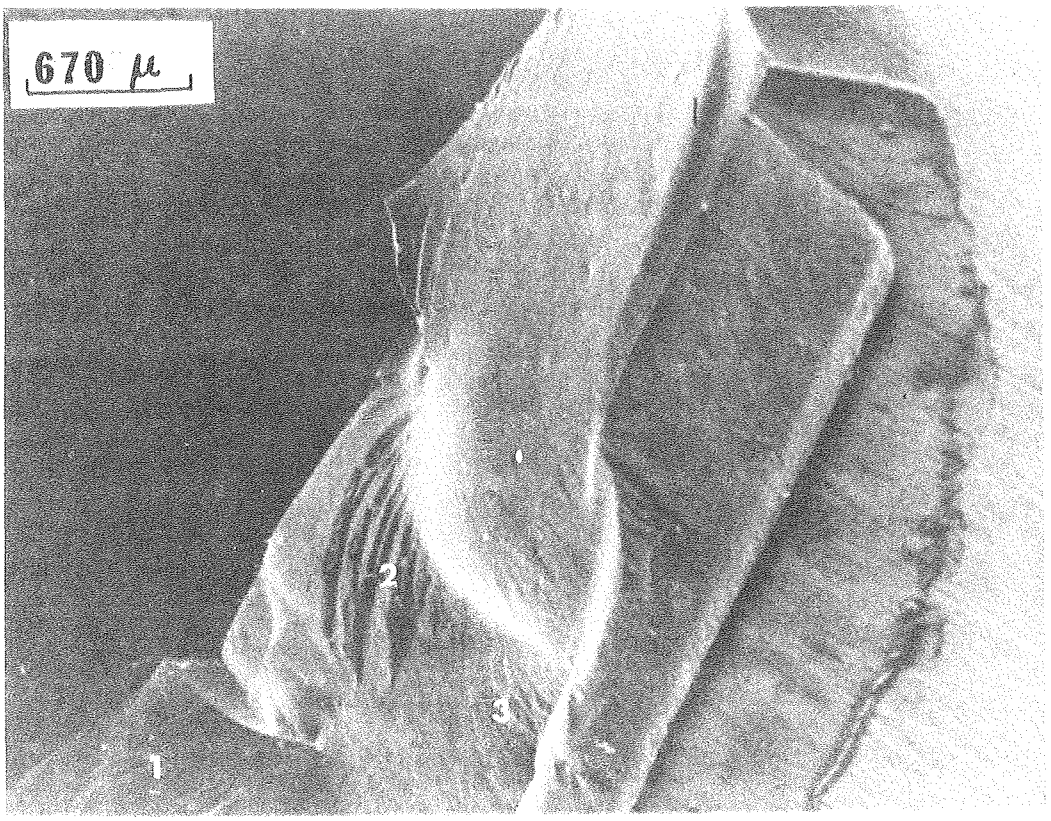

XBB776-5449

Fig. 31

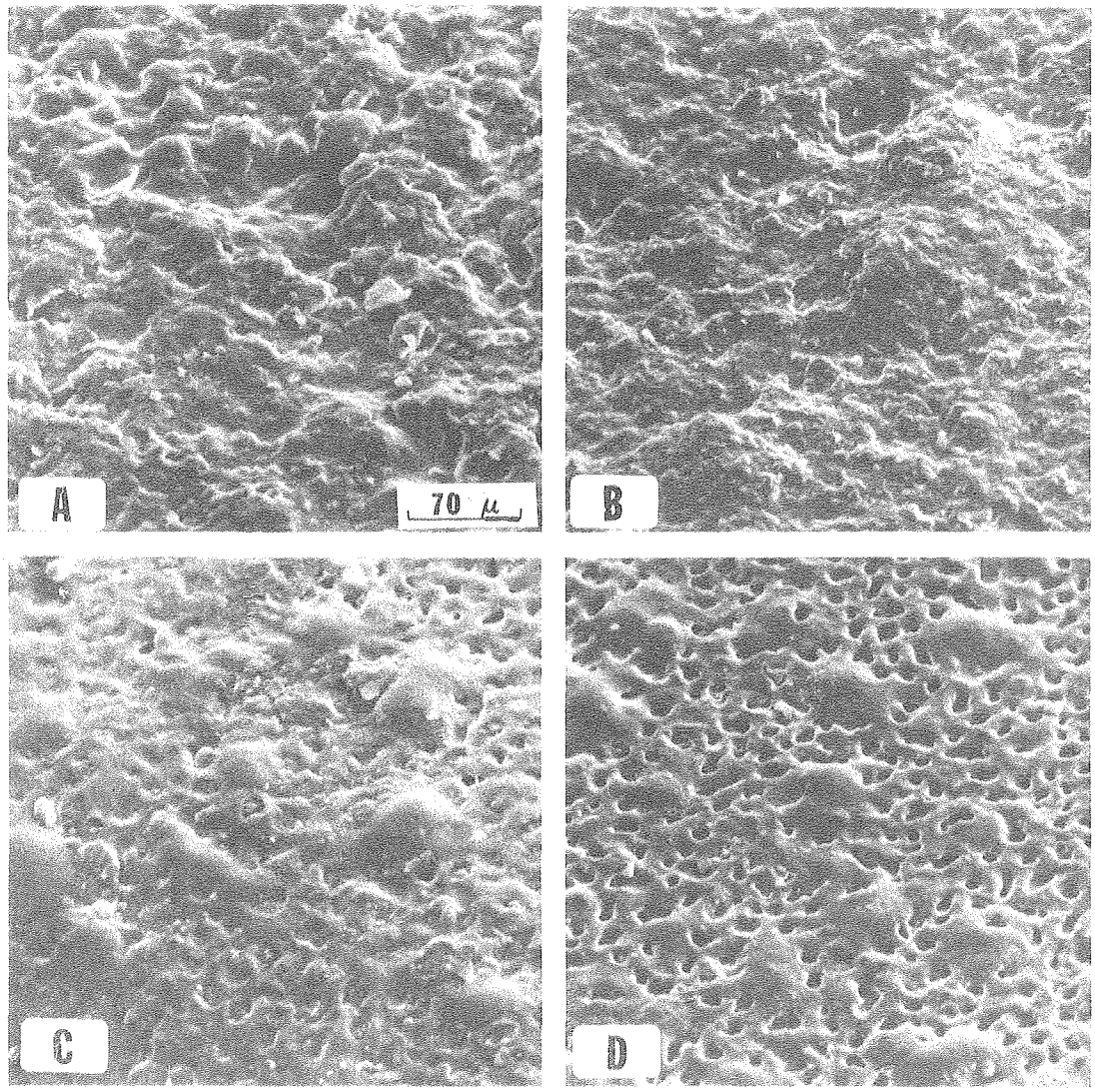

XBB776-5452

Fig. 32

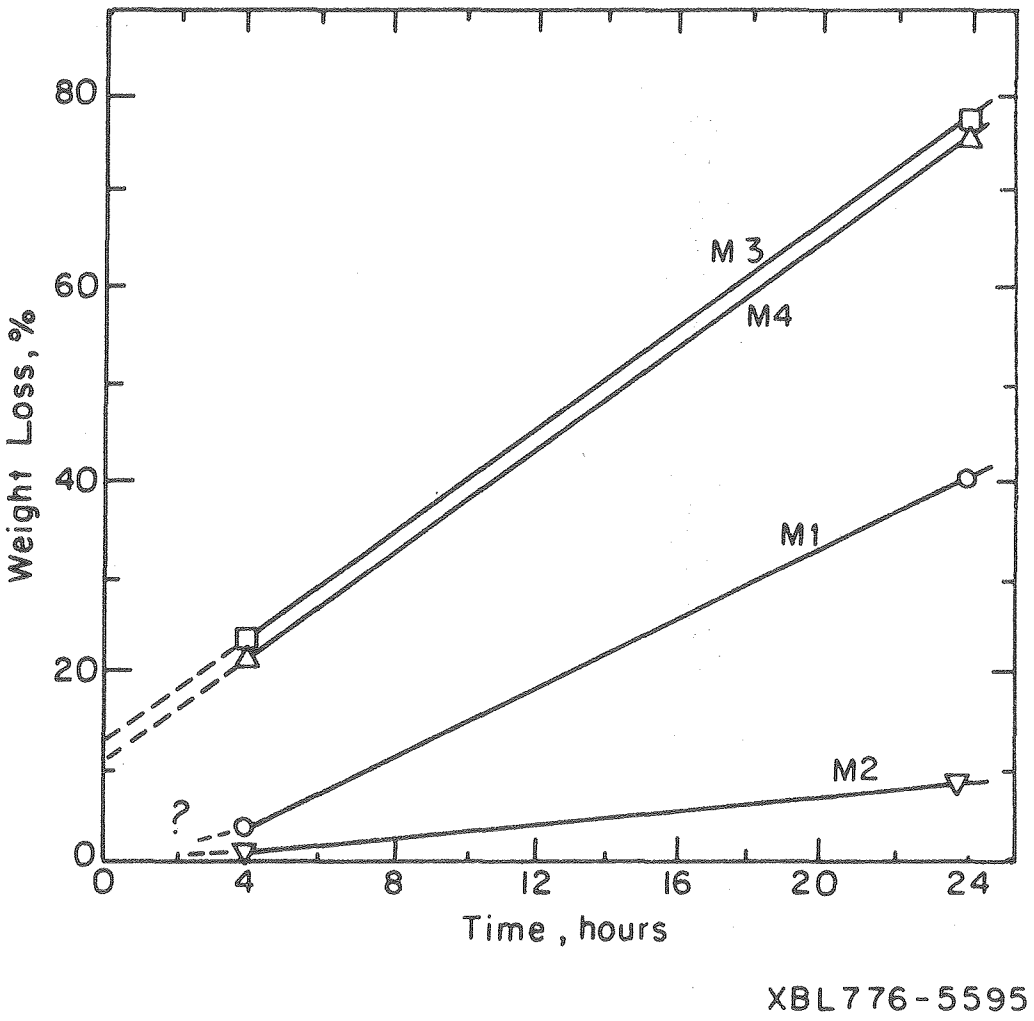
80
60
40
20
0
Weight Loss, %
0
4
8
12
16
20
24
Time, hours
M3
M4
M1
M2
?
XBL776-5595

Fig. 33

This report was done with support from the United States Energy Research and Development Administration. Any conclusions or opinions expressed in this report represent solely those of the author(s) and not necessarily those of The Regents of the University of California, the Lawrence Berkeley Laboratory or the United States Energy Research and Development Administration.